DESIGN OF A SERIES TILTING PAD BEARING AND SQUEEZE FILM DAMPER FOR NSF-TRC ROTORDYNAMIC TEST RIG AND ANALYSIS FOR OPTIMUM DAMPING AT BEARING SUPPORTS

by

Oscar De Santiago
Israel Silva
Dr. Luis San Andrés

May 1999

TRC-SFD-1-99

Texas A&M University
Mechanical Engineering Department

Design of a Series Tilting Pad Bearing and Squeeze Film Damper for NSF-TRC Rotordynamic Test Rig and Analysis for Optimum Damping at Bearing Supports.

TRC Project
Imbalance Response of a Rigid Rotor Supported on Series Tilting Pad Bearings and Integral Squeeze Film Dampers

By

Oscar C. De Santiago
Ph. D. student
Israel Silva
Undergraduate student
Luis San Andrés
Principal Investigator
Associate Professor

A Research Progress Report to the
Turbomachinery Research Consortium

TRC-SFD-1-99

May 1999

Design of a Series Tilting Pad Bearing and Squeeze Film Damper for NSF-TRC Rotordynamics Test Rig and Analysis for Optimum Damping at Bearing Supports.

TABLE OF CONTENTS

LIST OF TABLES

LIST OF FIGURES

NOMENCLATURE

c	*ISFD* radial clearance [0.229 mm, 0.009 in]
c_b	Tilting pad bearing assembly radial clearance [0.076 mm, 0.003 in]
c_p	Tilting pad bearing pad radial clearance [0.127 mm, 0.005 in]
C	Damping coefficient for the cylindrical mode [N-s/m (lbf-s/in)]
D	Bearing nominal diameter at pivot location [30.150 mm, 1.187 in]
e	Steady state rotor journal eccentricity [m, (in)]
f	Frequency ratio ω/ω_n
i	$\sqrt{-1}$
K	Stiffness coefficients for the first, cylindrical mode of vibration [N/m, (lbf/m)]
L	Damper land axial length [23.0 mm, 0.910 in]
L_b	Bearing pad axial length [22.86, 0.900 in]
m	Imbalance mass attached to rotor middle disk [gr.]
M	Rotor modal mass for the first mode of vibration [43.5 kg, 95.8 lbm]
N	Shaft speed (rps)
P	Tilting pad bearing unit load = W/L_bD (Pa)
r	Rotor middle disk radius for location of imbalance masses [114.3 mm, 4.5 in]
r_p	Tilting pad bearing preload c_p - c_b [mm, (in)]
R	*ISFD* journal radius [48.15 mm, 1.896 in]
R_s	Rotor shaft radius at bearing location [29.997 mm, 1.181 in]
S	Sommerfeld number = $S=\left(\frac{R_s}{c_p}\right)^2 \frac{\mu N}{P}$
u	$= m \bullet r/M$, Imbalance distance [m (in)]
W	Bearing static load [N (lb)]
x_b	Bearing (*ISFD* journal) steady state response [m(in)]
x	Rotor steady state synchronous response [m (in)]
Z	$= K + i\,\omega C$, Impedance function [N/m (lb/in)]
α	K_b / K_s , Bearing to support stiffness ratio
β	C_b / C_s , Bearing to support damping ratio
ε	$= e/c_b$, Dimensionless rotor journal eccentricity
ϕ	Attitude angle of steady state rotor center position within journal bearing [deg]
γ	$= K_{sV} / K_{sH}$, Ratio of vertical and horizontal support stiffness
μ	Lubricant viscosity [Pa-s]
ω	Frequency of excitation force and synchronous with rotor speed [rad/s]
ω_n	Rotor bearing system natural frequency [rad/s]
χ	Complex amplitude of rotor response
χ_b	Complex amplitude of the bearing response
ζ	System damping ratio

Subscripts

s	Refers to support properties
b	Refers to bearing properties
ind	Individual support property
eq	Equivalent property
opt	Optimum value
V, H	Vertical, horizontal direction
max	Maximum value of subindexed variable
xx,yy,	Rotordynamic coefficients direction
xy,yx	*x* vertical direction downwards, *y* horizontal direction to the right
E	Equivalent "static" property

Design of a Series Tilting Pad Bearing and Squeeze Film Damper for NSF-TRC Rotordynamics Test Rig and Analysis for Optimum Damping at Bearing Supports.

EXECUTIVE SUMMARY

Progress in the design and construction of a flexure pivot tilting pad journal bearing (*FPJB*) for imbalance response measurements in the NSF-TRC rotordynamic test rig is detailed. The *FPJBs* have been installed in series with existing integral squeeze film dampers (*ISFDs*). The combined supports replicate a configuration used on high performance compressors to reduce synchronous vibration problems and alleviate rotordynamic instabilities.

A design procedure was devised to render a bearing-damper support with optimum damping characteristics within the operating speed range to 10,000 rpm. Computed predictions based on a transfer matrix model show an improved vibration response of the test rotor mounted on the modified supports. Measurements of the synchronous test rotor response to calibrated imbalances will be conducted in the summer of 1999.

In addition, Appendix A details further identification of damping coefficients from impact response measurements conducted on the rotor mounted on integral dampers with tight (2 mil) end gap seals.

INTRODUCTION

High performance turbomachinery demands appropriate means to ensure structural isolation of components and stringent rotor vibration limits with tolerance to sudden imbalance loads due to blade loss events, shock and maneuver actions. Squeeze film dampers (*SFDs*) are the only effective means to reduce vibrations and to suppress instabilities in high performance aeroengine systems. Integral squeeze film dampers (*ISFDs*) offer distinct advantages such as reduced overall weight and length of the damper structure with less number of parts, accuracy of positioning (centering), and a split segment construction allowing easier assembly, inspection and retrofit than with any other type of damper. Flexure pivot tilting pad bearings offer similar construction features while minimizing (assembly) tolerances stack up and avoiding pivot wear and fretting. The series combination of a tilting pad bearing and a squeeze film damper has been implemented in numerous compressors to introduce flexibility and damping to the bearing

support. The proper design of these two mechanical elements allows for the optimum damping coefficient at the bearing support and accurate relocation of the (rigid mode) rotor bearing system critical speeds away from the operating speed range.

Measurements of imbalance responses of a test rotor supported on *SFDs* have been conducted since 1996. These experiments address to rotor-*SFD* configurations typical of aircraft gas turbines where safety and stability dictate the use of ball bearings instead of fluid film hydrodynamic bearings. This past year we proposed to perform measurements of the synchronous imbalance response of a test rotor supported on flexure pivot, tilting pad bearings and integral *SFDs*. The major objectives of the experiments are to determine the combined effect of the hydrodynamic bearings and *SFD*s on the location of critical speeds and effective logarithmic decrement, and to demonstrate the effectiveness of this bearing pair combination on reducing amplitudes of rotor vibration. The experimental results will allow benchmarking of predictive computational tools for estimation of force coefficients in both tilting pad bearings and squeeze film dampers.

AN APPRAISAL OF THE LITERATURE IN TILTING PAD JOURNAL BEARINGS

Cylindrical fluid film bearings are well known sources of self-excited rotor vibrations and induced by the cross-coupled forces from the lubricant film as a consequence of the dynamics of the shaft motion. Several bearing designs aim to alleviate this drawback of rigid pads cylindrical journal bearings by producing controlled changes in the film thickness distribution. Common geometry variations include multiple-lobe bearings, offset bearings, and pressure dam bearings. These bearings are capable of delaying the onset of instability to higher speeds than plain cylindrical journal bearings; and yet the destabilizing forces eventually appear under specific speed and load conditions.

The Tilting Pad Journal Bearing (*TPJB*) offers the distinctive advantage over fixed geometry bearings of suppressing the destabilizing forces due to the ability of the pads to conform to the adequate film thickness distribution when adequately designed. However, *TPJBs* present two major disadvantages: a) high sensitivity to pad geometry variations (due to load and temperature induced pad deformation), and b) stacking of manufacturing tolerances that greatly affect their steady state and dynamic performance characteristics (Zeidan and Paquette, 1994).

Hagg (1946) first demonstrates the ability of tilting pad journal bearings to suppress oil-induced instability in rotor-bearing systems. Hagg considers a balance of energy between the work performed by the oil film on the journal and the (viscous) damping energy dissipated by the oil film. The analysis is based on the assumption that a bearing pad adjusts its position about the pivot point under the action of the hydrodynamic pressure alone (i. e. no pivot friction or pad deformations are accounted for). The energy-balance analysis shows that a *TPJB*, as opposite to fixed geometry bearings, is not able to perform work on the journal, regardless of the mode of rotor vibration, thus rendering a stable bearing for any regime of operation. Experimental comparisons with similar sized fixed geometry bearings show that, for the regime of operation at which conventional bearings present oil whirling, tilting pad bearings (with 3, 4, 5, and 6 pads) remain stable for imbalance and impulse excitation forces.

Boyd and Raimondi (1953) perform an analysis of the *TPJB* using a simple approach. Each pad is considered to have a curvature such that, at the equilibrium condition, the pad acts as a plain slider bearing with a converging wedge. Further, all pads are (unrealistically) assumed to have the same leading to trailing edge thickness ratio. The load capacity as a function of the journal eccentricity, oil flow, and temperature raise is then easily determined for one pad. Finally, the contributions of all pads add together and render the overall bearing performance. A parametric study comparing full cylindrical journal bearings to *TPJBs* shows the tilting pad bearings to have smaller minimum film thickness and reduced power consumption (with smaller temperature raise of lubricant) for Sommerfeld numbers (S) greater than 20. The Sommerfeld number (S) for tilting pad journal bearings is defined as:

$$S = \left(\frac{R_s}{c_p}\right)^2 \frac{\mu N}{P}$$

where R_s is the shaft radius, c_p is the pad radial clearance, μ is the lubricant absolute viscosity, N is the shaft speed (in rev/s), and P is the bearing unit load (W/L_bD). Boyd and Raimondi regard *TPJBs* as disadvantageous since their load carrying capacity is smaller than that from similar cylindrical bearings.

The investigations by Hagg (1946), and Boyd and Raimondi (1953) render the steady state characteristics of *TPJBs* and point out to their ability as stability promoters. Hagg and Sankey (1956, 1958) perform controlled experiments of rotor response to imbalance and report damping coefficients of a *TPJB*.

Experimental tests demonstrate the ability of *TPJBs* to reduce rotor vibrations over a wide range of Sommerfeld numbers.

Lund (1964) defines stiffness and damping rotordynamic force coefficients for *TPJBs* using an assembly process adding the individual pad force coefficients. The analysis assumes the spring and damping coefficients for a fixed pad to be known a priori. These coefficients can be obtained by either analytical perturbation of the Reynolds equation or by numerical methods. Lund establishes the equation of motion for each pad introducing synchronous harmonic motions and including the pad mass moment of inertia. Coupling the equation of angular motion for the pad with the equations for the fluid film reaction forces yields the rotordynamic force coefficients for each pad. A parametric study for 4, 5, 6, and 12 pad *TPJBs* presents dimensionless stiffness and damping coefficients as a function of Sommerfeld numbers ranging from 0.1 to 10. Stiffness coefficients consistently decrease as the Sommerfeld number increases. In contrast, damping coefficients decrease slightly for low Sommerfeld numbers, but increase for larger Sommerfeld numbers.

Lund (1964) also demonstrates the importance of pad preload in increasing the rotordynamic (stiffness and damping) force coefficients. Pad preload is defined as the difference between the bearing assembly radial clearance and the pad machined radial clearance. Lund demonstrates that preloading the bearing pads results in bearing force coefficients up to two orders of magnitude larger than for zero-preload bearings. Comparisons with experimental damping coefficients show good agreement for a Sommerfeld number ranging from 0.1 to 10. However, experiments evidence increasing stiffness coefficients for increasing Sommerfeld numbers, as opposed to the theoretical predictions. Nonetheless, agreement of measurements and predictions is fairly good in the low Sommerfeld number range, 0.1 to 1.

A complete analysis of *TPJBs* should also account for thermal and elastic deformations of the pad since the bearing performance is greatly influenced by the film thickness distribution along the pads. Ettles (1980) introduces a computational analysis to evaluate bearing performance considering pad thermal and elastic effects. The Reynolds equation for the pressure distribution is coupled to the solution of the energy equation and elastic deformation equation on each pad. An iterative process renders the solution of the three equations for the bearing steady-state and dynamic force characteristics. The numerical predictions indicate that the major impact of the pad deformation is in the substantial reduction of the effective bearing

damping, where the difference with an isothermal rigid pad model can be of up to 60 %. Desbordes et al. (1994) implement an isothermal model to study the influence of pad elastic deformations using a finite element model. The numerical predictions confirm the result of bearing reduced damping coefficients, rendering increased rotor orbit amplitudes (20 % larger) compared to the orbits obtained for rigid pads.

Tilting pad journal bearings rely on the pads' natural tilting mechanism to provide their stabilizing feature. This mechanism is either a sliding friction element (spherical pivot) or a rolling friction element (rolling back-type pad). The pad support pivot connection has an inherent structural stiffness that modifies the film thickness distribution under operating conditions, especially for heavily loaded bearings. Kirk and Reedy (1988) study the influence of pivot stiffness on the performance of spherical- and line-pivoted pad bearings. Hertzian contact stress and deformation theory allows the derivation of expressions for an equivalent nonlinear pivot stiffness. Solution of the pressure distribution renders similar results as those obtained for the case of elastically deformed pads, i.e. pivot flexibility can reduce bearing damping coefficients by as much as 70 % in the case of spherical pivots of small radius.

The Electro Discharge Machining (EDM) process enables the pads to be integral to the bearing housing substituting the traditional pivot support by thin flexible beams (webs) attaching the bearing pads to the housing. The tilting effect is possible since the rotational (angular) stiffness of the web is very small. Accurate design of the web based on finite elements is essential to attain sufficient structural stiffness (so as to avoid fatigue and/or structural damage to the web or pad) while still allowing (free) tilting motions of the pad. Making the web beams increasingly rigid (larger cross section) makes the **F**lexure **P**ivot tilting pad **J**ournal **B**earing (*FPJB*) to evolve towards a fixed geometry fluid film bearing, thus increasing the cross-coupled stiffness coefficients which originate the destabilizing forces.

De Choudhury et al. (1992) present an early application of *FPJBs* to a high speed centrifugal compressor. Comparisons with similar sized conventional *TPJBs* show that the *FPJB* gives a reduced temperature raise and power loss. Yet, the rotor bearing system remains stable for the entire speed range of operation. The work addresses the importance of custom design of the pivot webs to optimize the rotor response and to accurately relocate the rotor critical speeds.

Several geometric factors affect the performance of *FPJBs*, namely pad circumferential position with respect to the load, pad preload and pivot offset, and others. Zeidan and Paquette (1994) thoroughly discuss

the effects of these parameters on the performance of conventional *TPJBs* and *FPJBs*. The authors conclude that, aided by the flexibility of the manufacturing process, *FPJBs* can provide a wider range of stiffness and damping coefficients than any other type of bearing configuration.

Chen (1994) presents a general method for calculation of the rotordynamic force coefficients for *FPJBs* including pivot flexibility and pad inertia. The radial stiffness of the supporting web affects directly the effective stiffness and damping of the bearing. As in conventional *TPJBs*, a low radial pad support (web) stiffness can lower the bearing damping coefficients, making the rotor-bearing system more sensitive to destabilizing forces from other sources. Zeidan (1992) shows that the pivot beam rotational stiffness modifies also the direct bearing stiffness coefficients, thus becoming an additional factor to be accounted for in the design of *FPJBs*.

San Andrés (1996) presents a computational analysis of the steady state and dynamic characteristics of flexure pivot bearings that accounts for fluid inertia and flow turbulence. These effects are of importance in extreme applications, such as high speed, high performance compressors and cryogenic fluid turbopumps. Walton and San Andrés (1997) report controlled experiments on the steady state characteristics of a flexure pivot tilting pad journal bearing tested in a vertical rotor rig and subjected to different loads and shaft speeds. Comparisons of bearing eccentricity measurements and numerical predictions show excellent correlation for the range of Sommerfeld numbers between 5 and 30. The experiments also evidence minimal cross-coupled forces. Computed predictions underestimate the experimental power losses, especially for larger Sommerfeld numbers (higher speeds and smaller loads). The experiments also reveal that the (dissipated) mechanical energy is mainly carried away by the lubricant film convection. Very little of the energy is heat-conducted through the bearing pads or the shaft, thus stressing the importance of the lubricant feeding mechanisms.

Tilting pad journal bearings may provide too large stiffness coefficients and could inhibit the effective action of the damping coefficients to control shaft vibrations. Many turbomachines such as process compressors, centrifugal pumps and steam turbines rely on *TPJBs* to avoid bearing destabilizing forces. There is the need for additional amounts of damping in high speed flexible rotors to ensure rotor stability under stringent operating conditions, seal and aerodynamically induced destabilizing forces, or even an eventual blade loss. Zeidan (1993, 1995) incorporating squeeze film dampers (*SFDs*) supports in series

with *FPJBs* has been able to stabilize marginally stable rotors operating on *TPJBs*. Squeeze film dampers provide the required amount of damping to maintain rotor stability as well as low (force) transmissibility to the rotor base.

Squeeze film dampers are mechanical components able to dissipate (viscous) energy from rotating structures due to the squeezing action of a whirling, non-rotating cylindrical journal within an annular lubricant film. Usually a rolling element bearing connects the inner journal to the rotating shaft, and a mechanical spring (squirrel cage) prevents journal rotation and centers it within a bearing housing. The squirrel cage may take up to three or four times as much axial space as the damper film land itself. The electro-discharge machining process allows the integral construction of the centering spring within the damper land axial length, enabling accurate centering of the rotating parts and facilitating a split construction for easiness of installation and retrofit.

De Santiago et al. (1997) present experiments on integral squeeze film dampers (*ISFDs*) supporting a three disk rigid rotor and subjected to rotating loads induced by calibrated imbalance masses. Measurements of the rotor synchronous response demonstrate the ability of the *ISFDs* in attenuating the rotor response in the range of operation from rest to 10,000 rpm. De Santiago and San Andrés (1998) report further experiments with *ISFDs* incorporating end plate seals with calibrated clearances to enhance the damping capability of the test dampers. The particular construction of the centering springs enables the damper to consistently provide increasing damping coefficients for tighter seals and without a severe reduction in the through flow of lubricant to the damper land. This enables the *ISFD* to provide larger amounts of damping without large increments in the lubricant temperature.

Zeidan (1995) describes the application of flexure pivot tilting pad journal bearings in series with integral squeeze film dampers to eliminate subsynchronous vibrations of a long and heavy flexible rotor in a steam turbine. The tilting pad journal bearings replace the original cylindrical bearings and the squeeze film dampers are introduced to provide flexibility and vibration dissipation. In the original support configuration, the bearings located too close to modal nodes (points of null deflection) provide little effective attenuation to the rotor vibrations. Installation of squeeze film dampers in series with the flexure pivot tilting pad journal bearings introduces flexibility to the bearing support and provides the required energy dissipation to safely operate the engine over the entire operating speed range. The adequate design

of the integral damper structural stiffness gives control for convenient relocation of the system critical speeds. The optimum amount of damping from the squeeze film dampers must be carefully assessed, for low values of support damping may not be sufficient to control rotor vibrations, whereas too large values of damping may lock the support and reduce its effective damping.

The current investigation aims to provide a reliable experimental database to confirm the benefits of the integral squeeze film damper-flexure pivot tilting pad journal bearing support combination in stabilizing and reducing the vibration of a massive test rigid rotor subjected to rotating loads generated by calibrated imbalance masses. Two identical four-pad flexure pivot tilting pad journal bearings in series with open-ends integral squeeze film dampers support a small gas turbine-sized three disk rotor. This report details the design process of the flexure pivot tilting pad journal bearing for optimum effective damping of the bearing-damper support combination.

DESCRIPTION OF TEST RIG AND INSTRUMENTATION

Figure 1 presents a view of the rig foundation and apparatus for testing of the *ISFD-FPJB* combination. The foundation is a 915 x 1220 x 216 mm (36 x 48 x 8.5 inch) metal-reinforced concrete table supported on four steel legs and set upon a 12.7 mm (0.500 in) steel plate separated from the laboratory floor by a polymer mat. The concrete table is covered by a 12.7 mm (0.500 in) desktop steel plate, upon which the test apparatus and the driving motor are placed.

The test apparatus consists of a variable speed DC drive motor, a 25.4 mm (1.000 in) steel base plate supporting two bearing pedestals, a midspan support for displacement sensors and the test rotor. A steel sheet container collects waste lubricant and redirects it to a waste sump. The apparatus steel base plate is elevated from the desktop plate by four threaded rods and leveling nuts and washers. An elastomeric foam material isolates vibration from the apparatus base plate to the desktop plate. A steel guard covers the apparatus during the imbalance tests providing safety and noise isolation.

The bearing span of the test apparatus is 406.4 mm (16 in). The bearing pedestals accommodate the test dampers in circumferential grooves of 126 mm in diameter and 35.94 mm long (dia.4.961 x 1.415 inch). The grooves become plenums for the lubricant supply into the dampers after installation of a damper-bearing assembly. The pedestals incorporate inlet and return ports with quick-lock connections. A single

inlet port is located on the top side of each pedestal and two drain conduits are located on each side of the bearing pedestals. Plexiglas covers on the outboard sides of the pedestals allow visualization of the damper and bearing assembly. Aluminum plate covers close the pedestals cavity on the inboard sides. Custom hose-type cylindrical seals prevent the lubricant axial leakage to ambient at the pedestal-shaft locations, while providing minimum additional structural damping (see De Santiago et al., 1997). Pressure gauges installed on each pedestal measure the inlet oil static pressure at the feeding grooves.

A 7.5 KW (10 HP) variable speed DC motor drives the test rotor to a maximum speed of 10,000 rpm. A flexible damped support holds and isolates the motor from the desktop plate supporting the test rig. A flexible coupling connecting the driving motor and the test rotor also isolates the rotor-bearing assembly from the vibration produced by the motor. A 250 Amp power supply controls the motor speed and is able to bring the rotor to its top speed within a few seconds. A drawn cup roller clutch connects the motor to the coupling and allows the rotor to spin freely when the power is shut off to the driving motor. An electrical blower automatically cools the motor when the temperature of the motor housing exceeds 46°C (115°F).

Figure 2 depicts the test rig lubrication system. ISO VG 10 oil contained in a 151 liter (40 gal) reservoir is fed into the bearings and dampers by means of a (gear-type) positive displacement pump driven by a variable speed motor. A return pump forces the lubricant from the bearing pedestals back into the reservoir. A set of valves directs the lubricant into the test rig at the selected inlet pressure, and an electrical heater and cooler keep the lubricant at any preset temperature. The main lubricant line feeds the dampers' film lands, while an additional line provides lubricant to the tilting pad bearings. These conduits were used in prior experiments for separate lubrication to support ball bearings.

The test rotor shown in Figure 3 has a mass (M) of 43.54 kg (95.9 lbs) and a length of 685.8 mm (27 inch). The rotor consists of a steel shaft of 76.2 mm (3 inch) in diameter, with 22.23 mm (0.875 in) diameter extensions in both ends. The rotor has three equally spaced 25.4 mm (1 inch) thick disks press-fitted onto the shaft. The drive end and middle disks have a diameter of 279.4 mm (11 inch), while the free end disk has a diameter of 228.6 mm (9 inch). Twelve equally spaced threaded holes of diameter equal to 4 mm (5/32 inch) in each disk allow installation of imbalance weights at constant radii of 114.3 mm (4.5 inch, large disks) and 76.2 mm (3.0 inch, smaller disk). The rotor shaft has a diameter of 25 mm (0.984 inch) at the bearing locations with two hardened steel collars of diameter equal to 29.97 mm (1.18 inch)

press-fitted at the tilting pad bearing locations. These collars provide the sliding surface for the rotor during start up and low speed spinning. The test rotor and the coupling components have been individually balanced at an external commercial facility.

Figure 4 shows the current instrumentation installed on the test apparatus. Six Dymac D60® eddy current transducers (proximity probes) at the two inboard locations on the bearing pedestals and at the midspan support measure the rotor vibration in three axial planes and in two orthogonal directions. Two accelerometers installed at the bearing pedestals measure the support motions. K-type thermocouples register the room, driving motor, inlet, and outlet lubricant temperatures. Two digital turbine-type flow meters display the oil flow through the bearing pedestals, and an optical tachometer for the rotor speed provides a synchronous peak signal for phase measurements. Three oscilloscopes display the rotor orbits at the three axial locations and a FFT analyzer displays the frequency content of selected vibration signals.

A 120 MHz Pentium personal computer is used for data acquisition and analysis of the rotor response. The Bentley Nevada Data Acquisition Interface Unit (DAUI) and the ADRE for Windows® software record the rotor speed, vibration response at the six locations of measurement and support accelerations during coast down tests at fixed speed decrements of 50 rpm. The acquisition system also performs low speed runout compensation and baseline (zero imbalance) vector compensation.

De Santiago et al. (1997) and De Santiago and San Andrés (1998) detail experiments conducted on *open ends* and *sealed ends* integral squeeze film dampers (*ISFD*), respectively. The test damper shown in Figures 5 and 6 consists of an outer ring (damper housing) and an inner non-rotating ring (damper journal), and eight S-shaped structural springs (webs) connect the journal to the damper housing. The damper film lands are contained within four arc segments of 52° around the journal. The damper clearances are uneven so that the journal becomes centered once the springs deform due to the rotor weight

The damper has an outer diameter of 126 mm (4.961 inch). The film land axial length is equal to 23 mm (0.906 inch) and at a radius of 48.15 mm (1.90 inch). The clearance between the journal and the housing is 0.229 mm (0.009 in) once the damper takes the rotor static load. The damper housing has an outer circumferential groove with four 1.6 mm (0.0625 inch) diameter orifices for lubricant supply into the damper lands.

DESIGN OF THE TEST FLEXURE PIVOT TILTING PAD JOURNAL BEARING

The damper journal inner race accommodates the test bearing. De Santiago, et al (1997), and De Santiago and San Andrés (1998) originally used (large stiffness) ball bearings for a rigid connection between the rotor and the damper. In the current research, a flexure pivot tilting pad fluid film bearing (*FPJB*) replaces the rolling element bearing. Thus, an all-fluid film bearing support results as the series combination of the *FPJB* and the squeeze film damper, as shown in Figure 7.

The bearing assembly of the test rig consists of three parts: the bearing pedestals, the integral squeeze film dampers (*ISFDs*), and the flexure pivot tilting pad journal bearings (*FPJBs*). Hereafter, the *ISFD*-pedestal combination is referred as the "bearing support". Prior experiments by De Santiago et al. (1997) indicate the bearing pedestals to be considerably flexible. Table 1 shows the characteristic stiffness of each pedestal in the vertical and horizontal directions. The equivalent stiffness and damping coefficients of the *ISFD*-pedestal combination have been also fully characterized (De Santiago et al, 1997).

The objective of the *FPJB* design is to minimize the test rotor response to mass imbalance at the first critical speed for the given open-ends *ISFD*-pedestal support parameters. It is also an objective of the *FPJB* design to avoid severe relocation of critical speeds with respect to the original rotor-*ISFD*-pedestal assembly as shown in Table 1. Appropriate selection of the *FPJB* lubricant film stiffness and damping coefficients allows achievement of the design objectives.

Figure 8 depicts a schematic view of the test rigid rotor supported on the series supports (*ISFD-FPJBs)*. Figure 9 represents the rotor-bearing system for the first rigid rotor mode of vibration (cylindrical). The system is represented by the rotor mass (M), the bearings' masses (M_b) and the tilting pad bearing stiffness (K_b) and damping (C_b) coefficients acting in series with the supports stiffness (K_s) and damping (C_s) coefficients. Note that the two supports and bearings contribute equally to the rotor response, i.e., for the cylindrical mode, $K_b = 2K_{bind}$, $C_b = 2C_{bind}$, and, $M_b = 2M_{bind}$, where the subindex (*bind*) stands for individual tilting pad bearing properties.

The governing equations for the absolute rotor (x) and bearing (x_b) motions are, respectively:

$$M\ddot{x} + K_b x + C_b \dot{x} - K_b x_b - C_b \dot{x}_b = Mu e^{i\omega t} \qquad , i = \sqrt{-1} \tag{1}$$

$$M_b \ddot{x}_b + (K_b + K_s) x_b + (C_b + C_s) \dot{x}_b - K_b x - C_b \dot{x} = 0 \tag{2}$$

where M, M_b are the rotor and bearing masses, respectively, u is the imbalance distance of the rotor's center of gravity, ω is the whirl frequency synchronous with rotor speed, and dots mean derivatives with respect to time.

The bearings mass M_b can be neglected ($M_b < 0.5$ kg) since it is considerably smaller than the rotor mass ($M = 43.5$ kg). The rotor and bearing frequency responses are of the form

$$x = \chi e^{i\omega t} \tag{3}$$

$$x_b = \chi_b e^{i\omega t} \tag{4}$$

Equation (2) can be solved for (x_b) in terms of (x). Substituting (x_b) into equation (1) leads to a single equation for the rotor motion (x) as:

$$M\,\ddot{x} + K_{eq}\,x + C_{eq}\,\dot{x} = Mue^{i\omega t} \tag{5}$$

where the equivalent tilting pad bearing-support stiffness and damping coefficients are:

$$K_{eq} = \frac{(K_b K_s - C_b C_s \omega^2)(K_b + K_s) + \omega^2 (K_b C_s + K_s C_b)(C_b + C_s)}{(K_b + K_s)^2 + (C_b + C_s)^2 \omega^2} \tag{6}$$

$$C_{eq} = \frac{(K_b C_s + K_s C_b)(K_b + K_s) - (K_b K_s - C_b C_s \omega^2)(C_b + C_s)}{(K_b + K_s)^2 + (C_b + C_s)^2 \omega^2} \tag{7}$$

These coefficients can be represented by a mechanical impedance Z_{eq} as:

$$Z_{eq} = K_{eq} + i\omega C_{eq} = \frac{Z_b Z_s}{Z_b + Z_s} = \frac{K_s(\alpha + \beta 2\zeta)(1 + i f 2\zeta)}{[(1+\alpha) + i f 2\zeta (1+\beta)]} \tag{8}$$

where:

$$Z_b = K_b + i\omega C_b \qquad \text{(tilting pad bearing impedance)}$$

$$Z_s = K_s + i\omega C_s \qquad \text{(support impedance)} \tag{9}$$

and $f = \dfrac{\omega}{\omega_n}$ is the excitation frequency ratio. $\alpha = \dfrac{K_b}{K_s}$ and $\beta = \dfrac{C_b}{C_s}$ are the bearing to support stiffness and the bearing to support damping ratio, respectively. $\zeta = \dfrac{C_s}{2M\omega_n}$ defines the support damping ratio and $\omega_n = \sqrt{\dfrac{K_s}{M}}$ is the natural frequency of the rotor supported on the damper-pedestals only, i.e. rigid bearings.

The rotor response amplitude can thus be expressed in terms of the excitation and the equivalent impedance as:

$$\chi = \frac{Mu\omega^2}{Z_{eq} - \omega^2 M} \tag{10}$$

At the rotor-support (rigid bearing) system natural frequency ($f = 1$), the dimensionless rotor response as a function of the bearing to support damping ratio (β) is, by substituting equation (8) into (10) and at $f = 1$,

$$\frac{\chi}{u} = \frac{(1+\alpha)+i2\zeta(1+\beta)}{-[(2\zeta)^2\beta+1]+i2\zeta(\alpha-1)} \tag{11}$$

The rotor response can be minimized by an appropriate choice of the bearing damping coefficient (C_b) for fixed values of bearing stiffness (K_b), support stiffness (K_s) and support damping (C_s) coefficients. The value of the bearing to support damping ratio (β_{opt}) which minimizes the rotor response at $f = 1$ is obtained by making zero the derivative of equation (11) with respect to β. This procedure leads to:

$$\beta_{opt} = \frac{-B \pm \sqrt{B^2 - 4AC}}{2A} - 1 \tag{12}$$

with

$$A = (2\zeta)^2[1-(2\zeta)^2]$$

$$B = (2\zeta)^4 + 2(2\zeta)^2[-2\alpha - 1] + 1 \tag{13}$$

$$C = -A^2(\alpha+1)^2[1-(2\zeta)^2]$$

As an example, Figure 10 shows the predicted rotor-bearing system response for values of $\alpha = 2$, $\zeta = 0.2$, $M = 45$ kg, and different values of the bearing to support damping ratio (β). Equation (12) renders the amount of damping that minimizes the rotor response at $f = 1$ as $\beta_{opt} = 8.94$. Figure 11 depicts the dimensionless ($|x/u|$) rotor peak amplitude at $f = 1$ as a function of the bearing to support damping ratio β for the same values of stiffness ratio ($\alpha = 2$) and damping ratio ($\zeta = 0.2$). The graph evidences the optimum value of $\beta = 8.94$ that renders the minimum rotor response at the rotor-support (rigid bearing) natural frequency.

At any given frequency, the complex amplitude of the test rotor χ is given, by substituting equation (8) into (10)), as

$$\chi = uf^2 \frac{[(1+\alpha)]+i\,[2\zeta\, f\,(1+\beta)]}{[\alpha - f^2(1+\alpha+(2\zeta)^2\beta)]+i[(2\zeta\, f)(\alpha+\beta-f^2(1+\beta))]} \tag{14}$$

The motion of the bearing and damper inner ring assembly (x_b), i.e. the massless connection between K_b and K_s in Figure 9, is given by:

$$x_b = \chi_b\, e^{i\omega t} \tag{15}$$

with

$$\chi_b = uf^2 \frac{\alpha+i[f\,2\zeta\,\beta]}{[\alpha - f^2(1+\alpha+(2\zeta)^2\beta)]+i[(2\zeta\, f)(\alpha+\beta-f^2(1+\beta))]} \tag{16}$$

The amplitude of the relative motion between the journal and the bearing assembly is then:

$$\chi - \chi_b = uf^2 \frac{1+i[f\,2\zeta]}{[\alpha - f^2(1+\alpha+(2\zeta)^2\beta)]+i[(2\zeta\, f)(\alpha+\beta-f^2(1+\beta))]} \tag{17}$$

Figure 12 shows the bearing (and *ISFD* inner journal) frequency response amplitude for different values of the bearing to support damping ratio (β). The relative motion of the journal and bearing assembly for a bearing to support damping ratio of $\beta = 1$ is shown in the bottom graph. Increasing values of the damping ratio (β) reduce the relative motion amplitude between the journal and the bearing assembly, i.e. making the connection more "rigid".

Optimization of the bearing to support damping ratio has been shown for an excitation frequency ($f=1$) corresponding to the rigid bearing natural frequency. The optimum bearing to support damping ratio at any other frequency is given from derivation of equation (14) with respect to (β) by:

$$\overline{\beta}_{opt} = \frac{-\overline{B} \pm \sqrt{\overline{B}^2 - 4\overline{A}\,\overline{C}}}{2\overline{A}} \tag{18}$$

where:

$$\overline{A} = (2\zeta\, f)^2\,[(2\zeta\, f)^2 - 2f^2 + 1]$$

$$\overline{B} = (2\zeta\, f)^2\,[(2+2\alpha) - 2f^2(1-\alpha) + (2\zeta\, f)^2] - 2f^2(1+\alpha) + 2\alpha + 1 \tag{19}$$

$$\overline{C} = (2\zeta\, f)^2\,(2f^2\alpha - \alpha^2) + 2f^2\,\alpha(1+\alpha) - \alpha^2$$

Table 2 shows the results of a parametric study for different values of α and ζ. The predictions offer insight on the large difference for the optimum bearing/support damping ratio (β_{opt}) when required to minimize the response of the original rigid bearing-rotor ($f=1$) and that including the bearing flexibility

The difference is easily understood since to minimize the response of the rotor on the flexible bearing-supports requires of large amounts of damping. In the design of the flexure pivot journal bearing, the optimum bearing to support damping ratio (β_{opt}) is selected at $f = 1$.

Selection of stiffness for test flexure pivot tilting pad bearing

Prior measurements show the bearing supports (pedestals) have stiffness coefficients that are different in the vertical and horizontal directions, see Table 1. On the other hand, the integral squeeze film dampers show (both from design and test validation) a radial stiffness of 3.5 MN/m (De Santiago et al., 1997). Thus, the effective stiffnesses of the combined (pair) bearing pedestals and integral dampers are equal to $K_{sV} = 5.6$ MN/m, and $K_{sH} = 4.83$ MN/m in the vertical and horizontal directions, respectively.

An equivalent "static" stiffness for the bearing (*FPJB*) stiffness in series with the support effective stiffness is equal to

$$K_E = \frac{K_s K_b}{K_s + K_b} \tag{20}$$

In the present application, a proper value of the bearing stiffness is selected to reduce the pedestals' stiffness asymmetry and to avoid a large relocation of the rotor-bearing system critical speeds. Let

$$\frac{K_{EH}}{K_{EV}} = 1 \tag{21}$$

and for a fixed value of the bearing stiffness K_{bV}, define $\gamma = K_{sV}/K_{sH}$. The bearing stiffness in the horizontal direction K_{bh} that renders $K_{EV} = K_{EH}$ is equal to

$$K_{bH} = \frac{\gamma K_{bV}}{\gamma + \frac{K_{bV}}{K_{sH}}(1-\gamma)} \tag{22}$$

For example, for $\gamma = 1.16$, $K_{sH} = 4.83$ MN/m, and $K_{bV} = 27.56$ MN/m, the above formulation yields K_{bH} = 129.41 MN/m. and $K_{EV} = K_{EH}$ = 4.65 MN/m. Notice the strong bearing asymmetry required to assure beaaring-support isotropy, i.e. $K_{bV}/K_{bH} = \frac{1}{4.7}$.

The computer program *hydrotrcM©* is used to compute the values of the *FPJB* stiffness and damping coefficients from a four pad, load between pads, flexure pivot journal bearing. The fluid film model is

laminar with adiabatic thermal boundaries. Table 3 shows the geometry of the *FBJB*, lubricant properties and operating conditions.

Table 4 presents the calculated synchronous force coefficients for the flexure pivot tilting pad bearing. The predictions show that the maximum attainable bearing stiffness asymmetry ($K_{xx} \neq K_{yy}$) is on the order of K_{bV}/K_{bH} =1/1.08. However, these bearing stiffness coefficients yield an equivalent support stiffness asymmetry of K_{EV}/K_{EH} = 1.12, at 3,000 rpm.

Figure 13 depicts the final *FPJB* design including its significant dimensions for manufacturing. Figure 14 shows the predicted bearing journal eccentricity and attitude angle for the range of test operation (0 to 10,000 rpm). Figure 15 depicts the bearing synchronously reduced bearing stiffness and damping coefficients versus rotor speed. The bearing coefficients in the vertical and horizontal directions at 3,000 rpm are

Horizontal -	K_{yy} = 11.9 MN/m,	C_{yy} = 24.0 KN-s/m	
Vertical -	K_{xx} = 11.79 MN/m	C_{xx} = 24.2 KN-s/m	(single bearing)

These results yield bearing to support stiffness and optimum damping ratios of:

α_V = 4.21, $\beta_{opt\,V}$ = 21.2

α_H = 4.93, $\beta_{opt\,H}$ = 26.7

Table 1 includes the (measured) values of support damping, i. e. overall system damping for the open ends *ISFD* and bearing pedestals. Then, the bearing to support damping ratio is $\beta_{opt\,V} = C_{xx}/C_{sV}$ = 11.1 and $\beta_{opt\,H}$ = C_{yy}/C_{sH} = 15.34, in the vertical and horizontal directions, respectively. Thus, the selected tilting pad bearing is expected to provide damping coefficients that are smaller than those needed for optimum damping conditions.

The overall bearing assembly equivalent stiffness and damping coefficients are calculated using equations (6) and (7). Table 5 shows the equivalent series *FPJB* and *ISFD* stiffness and damping coefficients in the vertical and horizontal directions. Figure 16 depicts these coefficients as a function of the rotor speed.

PREDICTIONS OF THE IMBALANCE RESPONSE FOR THE TEST ROTOR SUPPORTED ON SERIES FPJBS AND ISFDS

The test flexure pivot bearing outer ring is to be press fitted into the existing integral damper inner diameter. Four pads are attached to the bearing outer ring by means of structural webs as depicted in Figure 13. The webs locate the pads and still allow for pad tilting motions since the rotational stiffness of the webs is low. The damper journal contains a circumferential groove for lubricant supply, and the bearing has four inlet ports of diameter equal to 2.54 mm (0.1 inch) to inject lubricant close to the pads' leading edges. The damper journal inner race diameter has been enlarged to 47.63 mm (1.875 inch) to better accommodate the *FPJB*. Table 3 summarizes the final *FPJB* geometric dimensions.

A 38 stations transfer matrix model predicts the imbalance response of the rotor-bearing system represented in Figure 17. Figure 18 shows the damped eigenvalue frequency map and the locus of the damping ratio for the different natural frequencies. The system is stable for the entire range of test speeds (0-10,000 rpm) as expected. Figure 19 depicts typical rotor imbalance response predictions in the three measurement planes (drive end, rotor end, and near middle disk) for a mass imbalance of 45 gr-in inserted at the rotor middle disk. Maximum amplitudes of rotor response at the critical speeds remain within 50% of the *ISFD* radial clearance. Figure 20 shows that the *ISFD-FPJB* combination renders smaller rotor orbit amplitudes at the critical speed than the orbit amplitudes for the rotor supported on *ISFD* and ball bearings only.

CLOSURE

Presently, the test bearings have been manufactured and installed in the *ISFD's* journal inner races. A special lifting mechanism is intended to suspend the rotor within the bearing clearance at rotational speeds below 1,000 rpm. This mechanism will aid the *FPJB* during start up and coast down for extended babbitt liner life and reduced start-up torque.

Rotor imbalance response measurements will be conducted once the lifting mechanism is completed and the lubricant lines modified to provide the required flow through the test bearings. The experiments

will be performed in the summer of 1999. The test schedule, procedure for measurements and parameter identification method are identical to those reported by De Santiago and San Andrés (1998).

ACKNOWLEDGEMENTS

The support of the Turbomachinery Research Consortium is gratefully acknowledged. KMC, Inc., is also recognized for providing feedback on the design and manufacturing of the test flexure pivot tilting pad journal bearings.

REFERENCES

Boyd, J., and Raimondi, A. A., 1953, "An analysis of the Pivoted-Pad Journal Bearing", *Mechanical Engineering*, Vol. 75, pp. 380-386.

Chen, W., 1994, "Bearing Dynamic Coefficients of Flexible-Pad Journal Bearings", *Proceedings of the ASME/ASLE Tribology Conference*, Lahaina, Hawaii, Preprint 94-TC-4D-1.

De Choudhury, P., Hill, M. R., and Paquette, D. J., 1992, "A Flexible Pad Bearing System for a High Speed Centrifugal Compressor", *Proceedings of the 21st Turbomachinery Symposium*, Dallas, Tx, pp 57-64.

De Santiago, O., Oliveras, J., and San Andrés, L., 1997, "Imbalance Response of a Rotor Supported on Integral Open Ends *SFDs*," Turbomachinery Research Consortium Annual Report, Texas A&M University, TRC-*SFD*-2-97, April.

De Santiago, O., and San Andrés, L., 1998, "Imbalance Response of Rotor Supported on Sealed Integral Dampers," Turbomachinery Research Consortium Annual Report, Texas A&M University, TRC-*SFD*-1-98, May.

Desbordes, H., Fillon, M., Wai, C. C. H., and Frene, J., 1994, "Dynamic Analysis of Tilting-Pad Journal Bearing - Influence of Pad Deformations", Transactions of the ASME, *Journal of Tribology*, July, Vol. 116, pp. 621-628.

Ettles, C. M. McC., 1980, "The Analysis and Performance of Pivoted Pad Journal Bearings Considering Thermal and Elastic Effects", Transactions of the ASME, *Journal of Lubrication Technology*, April, Vol. 102, pp. 182-192.

Hagg, A. C., 1946, "The Influence of Oil-Film Journal Bearings on the Stability of Rotating Machines", Transactions of the ASME, *Journal of Applied Mechanics*, Vol. 68, Sept., pp. A211-A220.

Kirk, R. G., and Reedy, S. W.,1988, "Evaluation of Pivot Stiffness for Typical Tilting-Pad Journal Bearing Designs", Transactions of the ASME, *Journal of Vibration, Acoustics, Stress, and Reliability in Design*, April, Vol. 110, pp. 165-171.

Lund, J. W., 1964, "Spring and Damping Coefficients for the Tilting-Pad Journal Bearing", *ASLE Transactions*, Vol. 7, pp. 342-352.

San Andrés, L., 1996, "Turbulent Flow, Flexure-Pivot Hybrid Bearings for Cryogenic Applications," ASME Journal of Tribology, Vol. 118, 1, pp. 190-200.

Walton, N., and L. San Andrés, 1997, "Measurement of Static Loading Versus Eccentricity in a Flexure-Pivot Tilting Pad Journal Bearings," ASME Journal Of Tribology, Vol. 119, 2, pp. 297-305.

Zeidan, F., 1992, "Developments in Fluid Film Technology", Turbomachinery International, Vol. 9, pp. 24-31.

Zeidan, F. Y., Perez, R. X., and Stephenson, E. M., 1993, "The Use of Honeycomb Seals in Stabilizing Two Centrifugal Compressors", *Proceedings of the 22nd Turbomachinery Symposium*, Dallas, Tx, pp 57-64.

Zeidan, F. Y., and Paquette, D. J., 1994, "Application of High Speed and High Performance Fluid Film Bearings in Rotating Machinery", *Proceedings of the 23rd Turbomachinery Symposium*, Dallas, Tx, pp 57-64.

Zeidan, F., 1995, "Application of Squeeze Film Dampers", *Turbomachinery International*, Vol. 11, September/October, pp. 50-53.

TABLES

Table 1. Mechanical parameters for integral dampers and pedestals.

Parameter		
Individual ISFD design structural stiffness	$K_{ISFDV} = K_{ISFDH} = 3.5$ MN/m	(20,000 lb/in)
Experimental (individual) pedestal stiffness	*Vertical:* Drive end ~ 30.7 MN/m Free end ~ 28.0 MN/m *Horizontal:* Drive end ~ 14.0 MN/m Free end ~ 10.2 MN/m	 ~ (175,000 lb/in) ~ (160,000 lb/in) ~ (80,000 lb/in) ~ (58,000 lb/in)
Experimental *ISFD*-pedestal (support) stiffness[1]	$K_{sV} = 5.59$ MN/m $K_{sH} = 4.83$ MN/m	(31,890 lb/in) (27,550 lb/in)
Experimental *ISFD*-pedestal-rotor system natural frequency	$\omega_{nV} = 352$ r/s (56 Hz) $\omega_{nH} = 327$ r/s (52 Hz)	
Experimental Rotor-*ISFD*-pedestal (rotor-support) critical speeds	*Vertical* = 3,200 – 3,450 rpm (51 Hz) *Horizontal* = 2,900 - 3,100 rpm (55 Hz)	
Average experimental system damping coefficients (open ends *ISFDs*, structural + viscous damping)[1]	$C_{sV} = 4{,}330$ N-s/m $C_{sH} = 3{,}130$ N-s/m	(24.87 lb-s/in) (17.85 lb-s/in)

[1]Values include the combined effect of two identical bearing supports in parallel acting in the cylindrical mode of vibration of the rigid rotor, from De Santiago, et al., 1997

Table 2. Parametric study of optimum bearing to support damping β_{opt} ratio for different values of rotor-support damping coefficient (ζ) and bearing to support stiffness ratio (α).

						x^* at $f = 1$ with $\beta = \beta_{opt}$				
ζ	α	ω/ω_n	$\omega/\omega_n\|_{xmax}$	β_{opt} *at* $f = 1$	$x^*_{max}/u\|\beta_{opt}$	x^*/u	x^*_b/u	$(x - x_b)^*/u$	*Relative Phase (deg)*	$\overline{\beta}_{opt}$ *for* $f\|_{xmax}$
0.10	2	0.82	0.86	*8.09*	3.24	2.62	1.96	0.74	-160	64.6
	4	0.89	0.94	*20.6*	3.65	3.44	3.01	0.52	-151	44.0
	6	0.93	0.98	*34.5*	3.94	3.68	3.55	0.39	-146	43.4
0.15	2	0.82	0.92	*8.4*	2.43	2.31	1.85	0.56	-154	18.1
	4	0.89	0.98	*19.8*	2.75	2.74	2.46	0.35	-145	23.5
	6	0.93	1.00	*31.8*	2.91	2.92	2.73	0.25	-142	31.8
0.20	2	0.82	0.96	*8.94*	2.03	2.02	1.70	0.41	-149	12.0
	4	0.89	1.00	*20.2*	2.24	2.34	2.06	0.24	-142	20.2
	6	0.93	1.02	*31.7*	2.33	2.32	2.12	0.17	-140	27.8

Table 3. Test bearing (*FPJB*) geometry and lubricant.

Nominal Diameter:	30.0 mm (1.181 in)
Length:	22.9 mm (0.902 in)
Number of Pads:	4
Direction of Load:	Load between pivots
Pad Radial Clearance:	127 microns (0.005 in)
Pad arc length:	72 deg
Preload:	0.405 (r_p = 50.8 microns, 0.002 mm)
Pivot offset:	0.55 (38.5 deg) in direction of rotation
Material:	Steel-babbit
Lubricant:	*ISO VG 10*
Dynamic viscosity μ:	14.8 cP @ 25° C
Bearing static carrying load:	214 N (48.0 lbf)
Web rotational stiffness:	40 N-m/rad

Table 4. Flexure pivot journal bearing synchronous rotordynamic coefficients.

x vertical downwards
y Horizontal to the right

Speed rpm	K_{xx} MN/m	K_{xy} MN/m	K_{yx} MN/m	K_{yy} MN/m
1000	19.4	4.96	3.59	19.5
2000	14.0	3.38	2.09	14.1
3000	11.8	2.89	1.58	11.9
4000	10.5	2.57	1.25	1.06
5000	9.68	2.44	1.07	9.81
6000	9.10	2.37	0.943	9.26
7000	8.66	2.33	0.847	8.85
8000	8.35	2.29	0.753	8.57
9000	8.08	2.28	0.695	8.34
10000	7.86	2.29	0.648	8.15

Speed rpm	C_{xx} (KN-s/m)	C_{xy} (KN-s/m)	C_{yx} (KN-s/m)	C_{yy} (KN-s/m)
1000	88.5	18.2	21.9	88.0
2000	38.0	7.01	9.12	37.7
3000	24.1	3.68	5.08	24.0
4000	17.1	1.93	3.16	17.2
5000	13.6	1.58	2.63	13.7
6000	11.3	1.40	2.28	11.4
7000	9.64	1.23	1.93	9.64
8000	8.59	1.05	1.75	8.44
9000	7.53	1.05	1.58	7.54
10000	6.83	0.877	1.40	6.84

Table 4 (continued). Flexure pivot journal bearing synchronous rotordynamic coefficients.

Speed Rpm	Dimensionless Eccentricity (x direction)	Dimensionless Eccentricity (y direction)	Dimensionless Eccentricity $\varepsilon = e/c_b$ (rounded)	Attitude angle ϕ (deg)
1000	0.707	0.0162	0.707	1.55
2000	0.637	0.0201	0.638	1.54
3000	0.586	0.0223	0.586	1.53
4000	0.545	0.0244	0.545	1.53
5000	0.509	0.0265	0.510	1.52
6000	0.479	0.0282	0.480	1.51
7000	0.451	0.0298	0.452	1.50
8000	0.427	0.0308	0.429	1.50
9000	0.406	0.0320	0.407	1.49
10000	0.386	0.0332	0.387	1.48

Table 5. Equivalent bearing-damper stiffness and damping coefficients in the range of 0 – 10,000 rpm.

Speed (rpm)	$K_{eq\,V}$ (MN/m)	$C_{eq\,V}$ (KN-s/m)	$K_{eq\,H}$ (MN/m)	$C_{eq\,H}$ (KN-s/m)
1000	2.48	2.93	2.18	2.19
2000	2.38	2.47	2.10	1.86
3000	2.31	2.24	2.05	1.69
4000	2.25	2.07	2.00	1.58
5000	2.20	1.96	1.97	1.50
6000	2.16	1.88	1.94	1.44
7000	2.13	1.81	1.92	1.39
8000	2.11	1.75	1.90	1.35
9000	2.08	1.70	1.88	1.31
10000	2.07	1.66	1.87	1.28

FIGURES

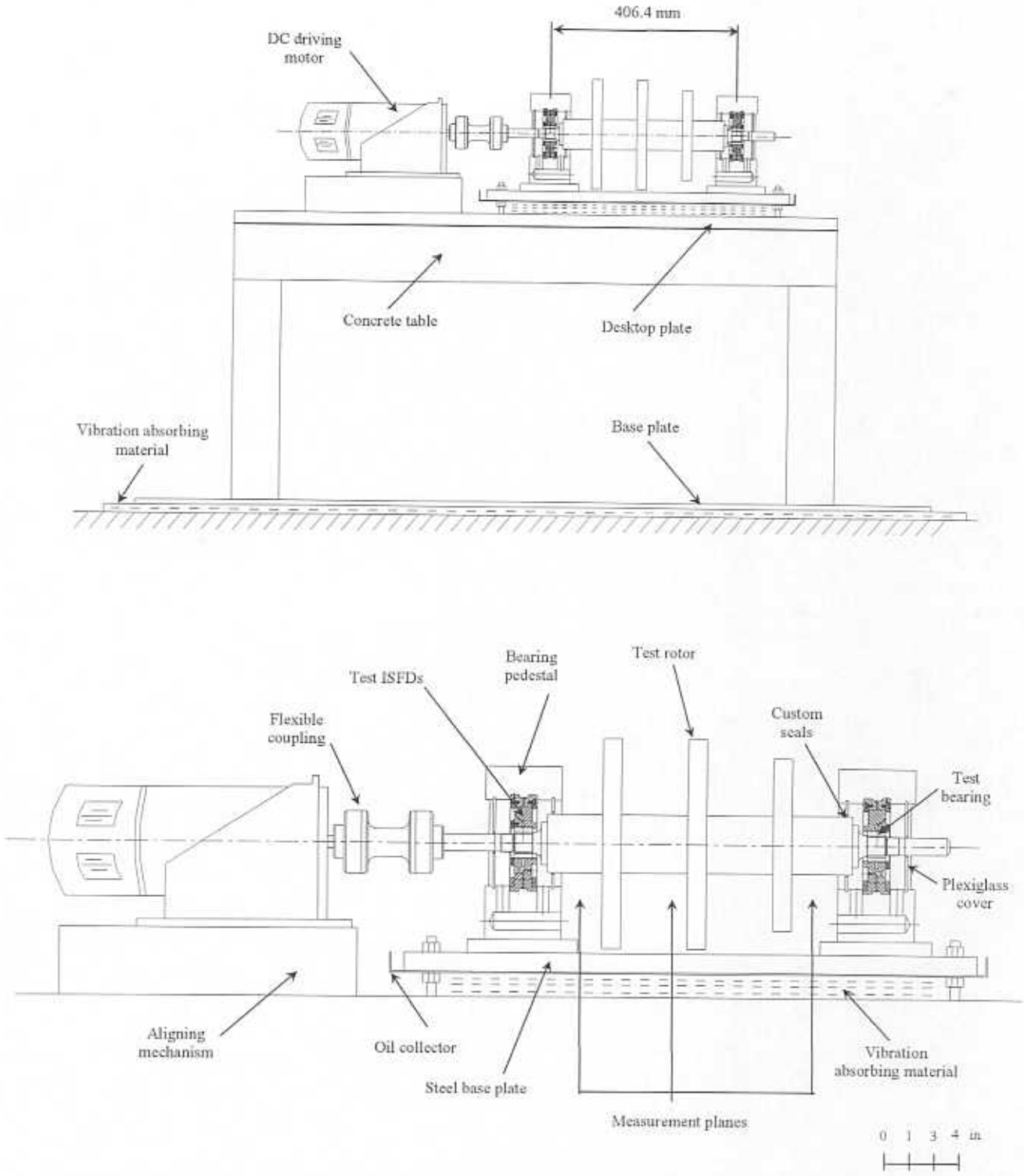

Figure 1. The test rig configuration for squeeze film dampers and test apparatus detailed construction.

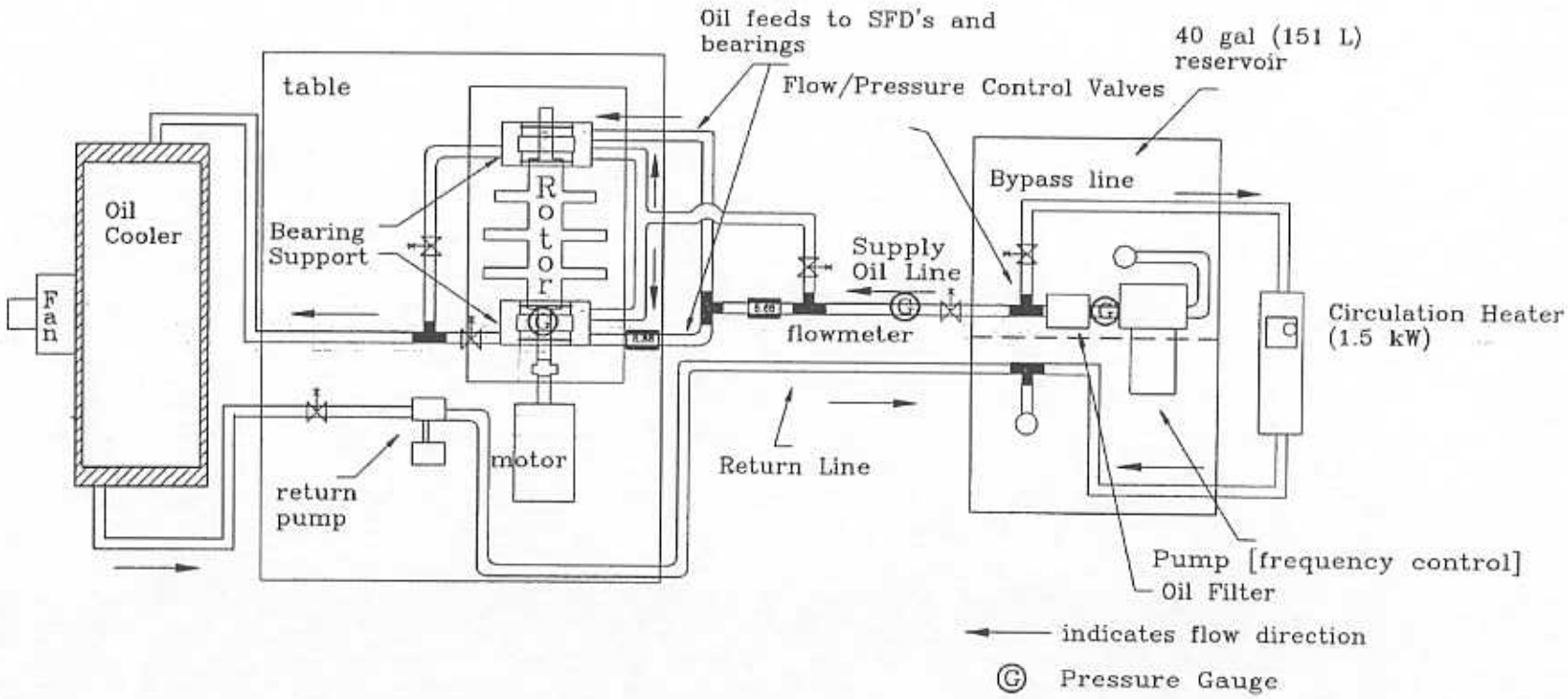

Figure 2. Lubrication system of squeeze film damper test apparatus.

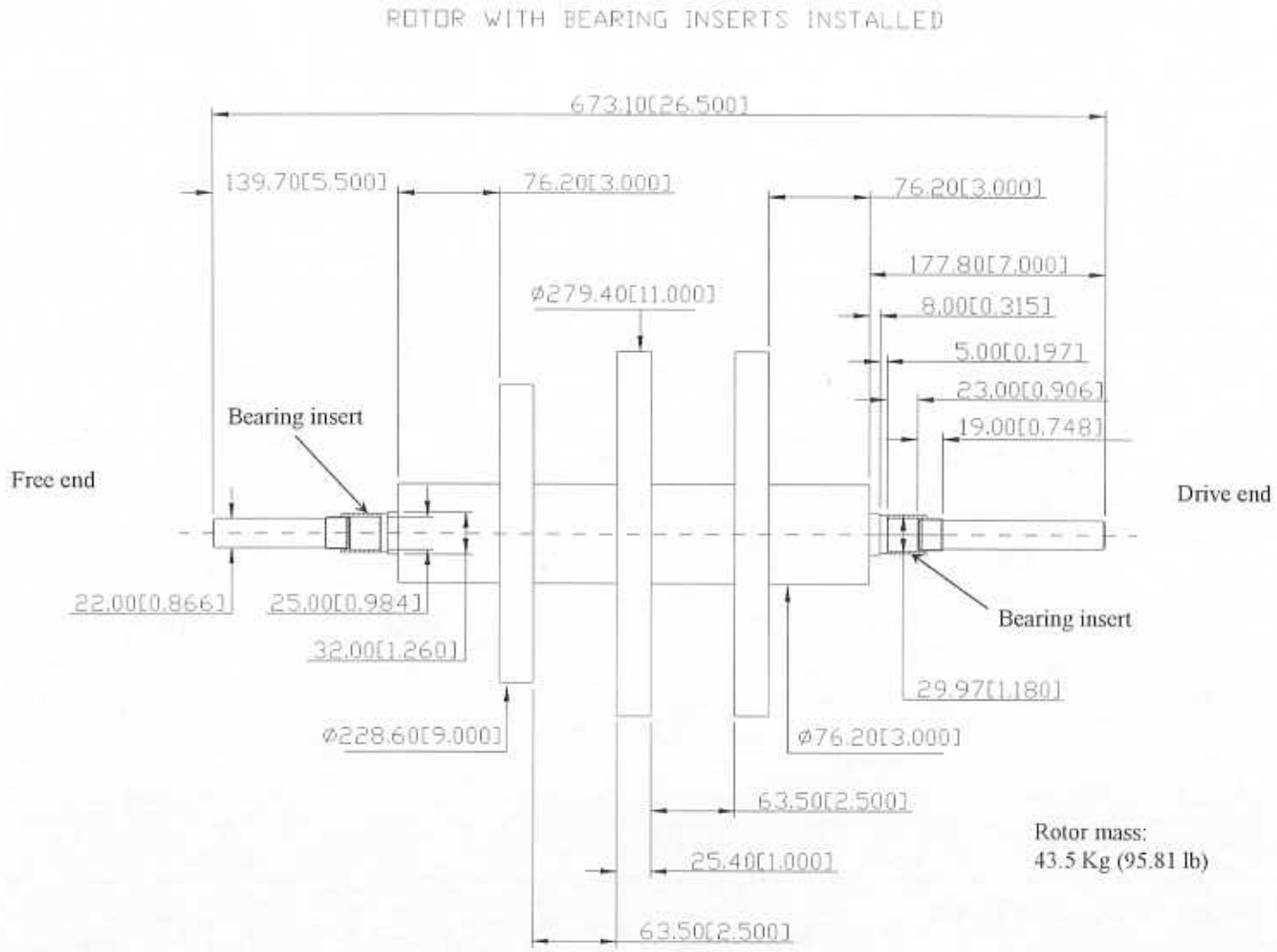

Figure 3. Test rotor main dimensions with hardened bearing races (steel inserts).

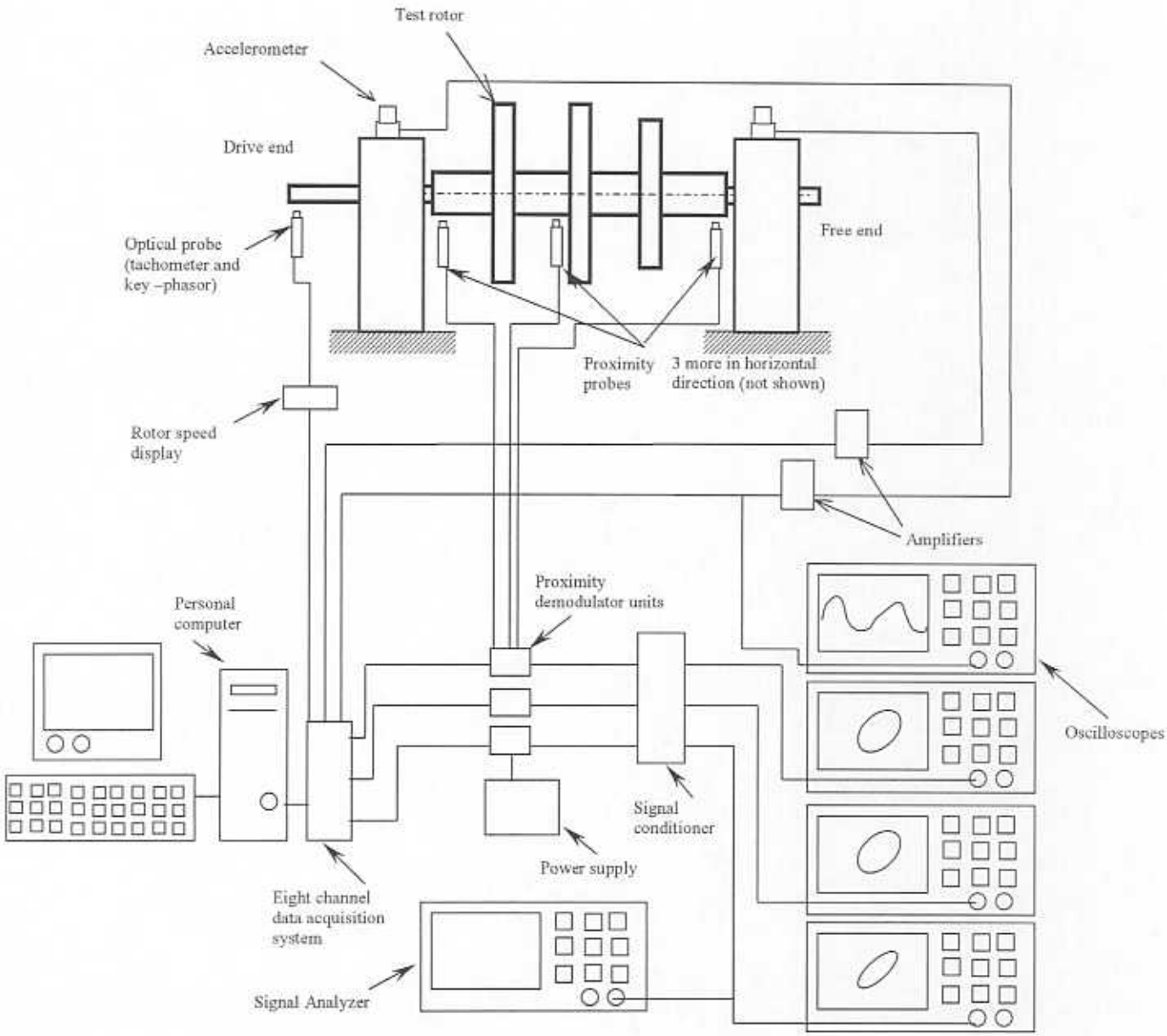

Figure 4. Instrumentation for rotor imbalance response measurements.

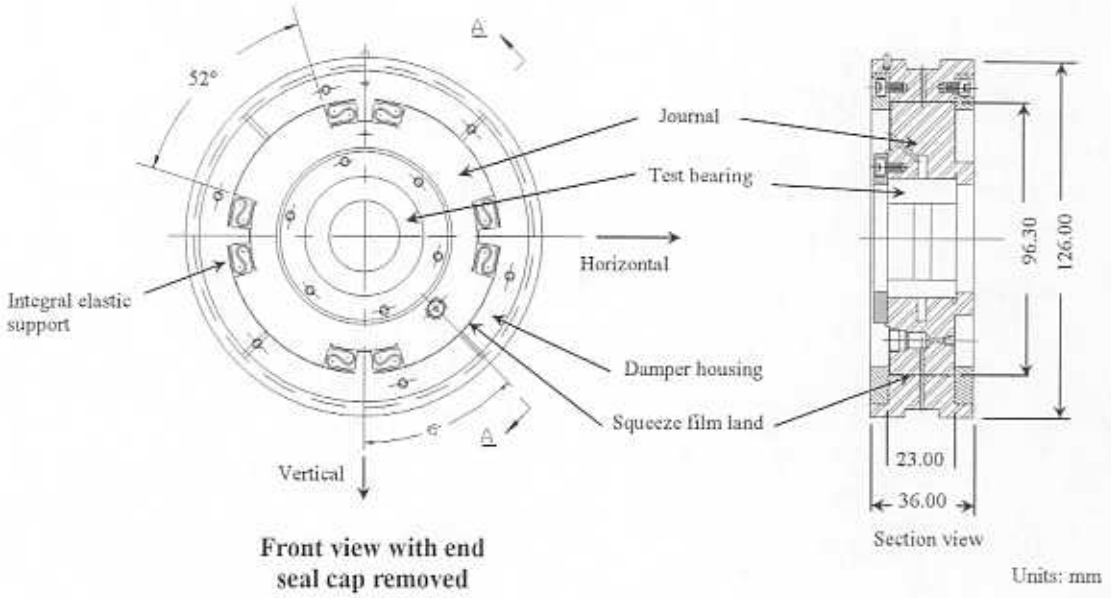

Figure 5. Test integral squeeze film damper.

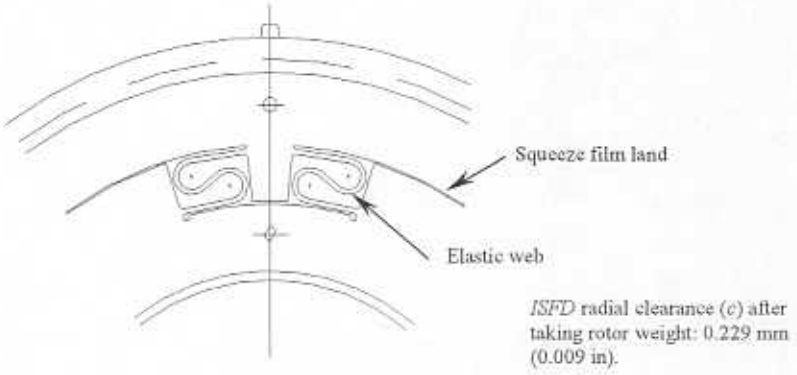

Figure 6. Detail of *ISFD* web construction.

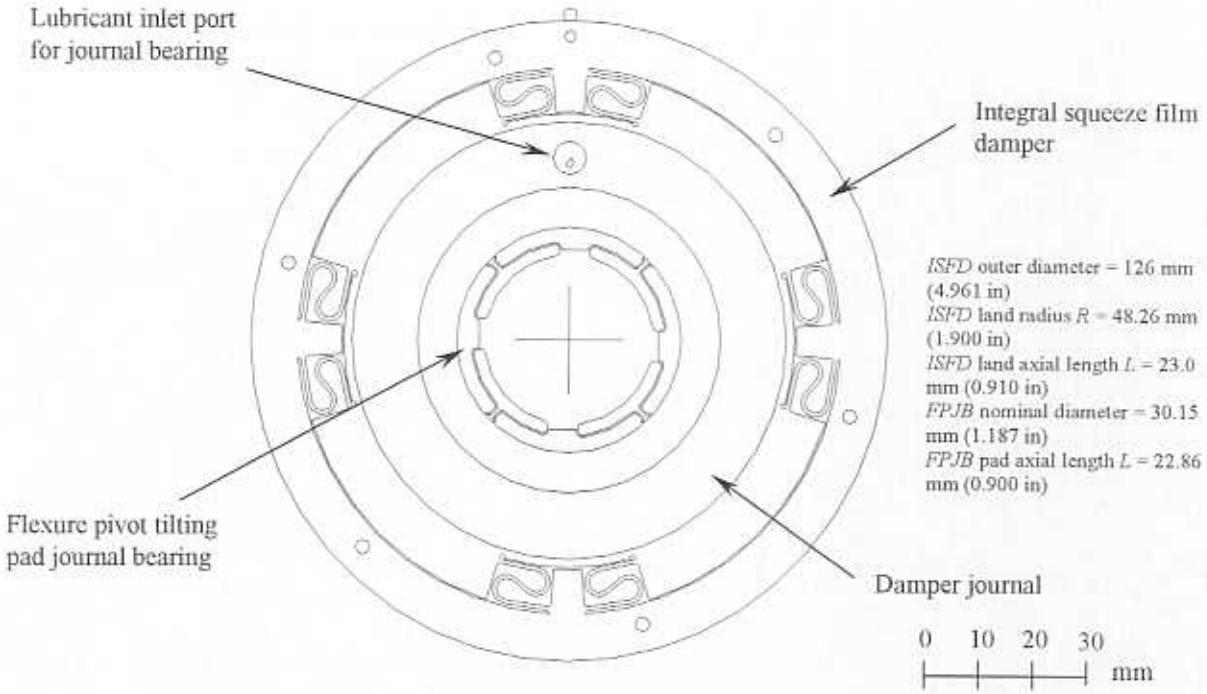

Figure 7. Integral squeeze film damper and flexure pivot tilting pad journal bearing assembly.

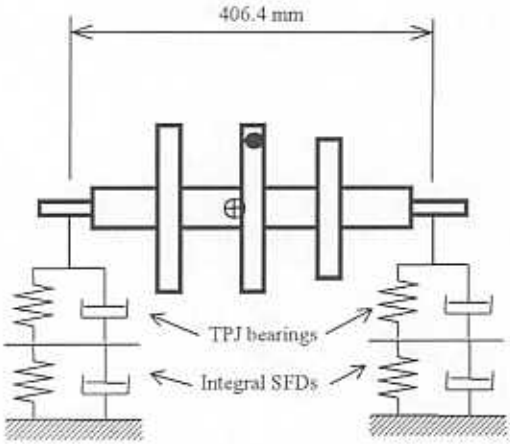

Figure 8. Three-disk rotor supported on tilting pad journal bearings in series with integral squeeze film dampers.

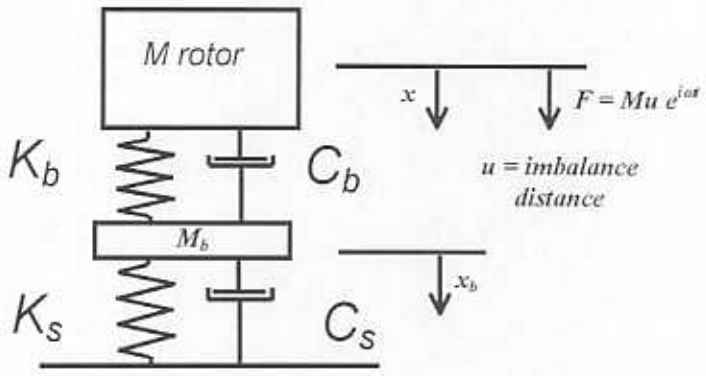

Figure 9. Simplified planar model for rigid rotor mounted on series *FPJBs* and *ISFDs*.

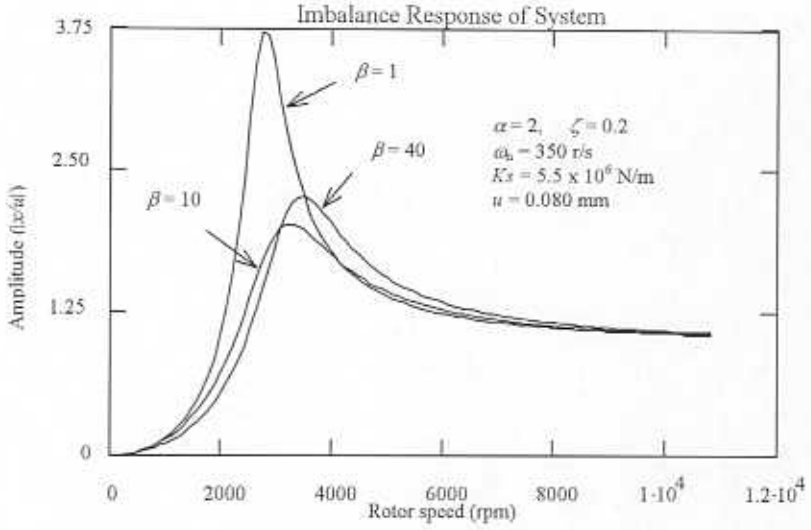

Figure 10. Dimensionless rotor imbalance response for different values of bearing to support damping ratios (β).

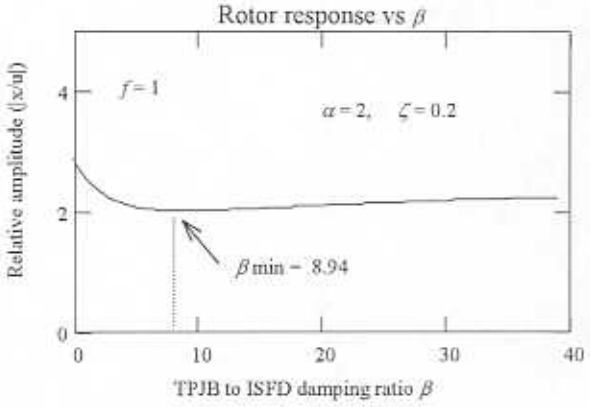

Figure 11. Dimensionless rotor peak amplitude at $f = 1$ as a function of bearing to support damping ratio (β).

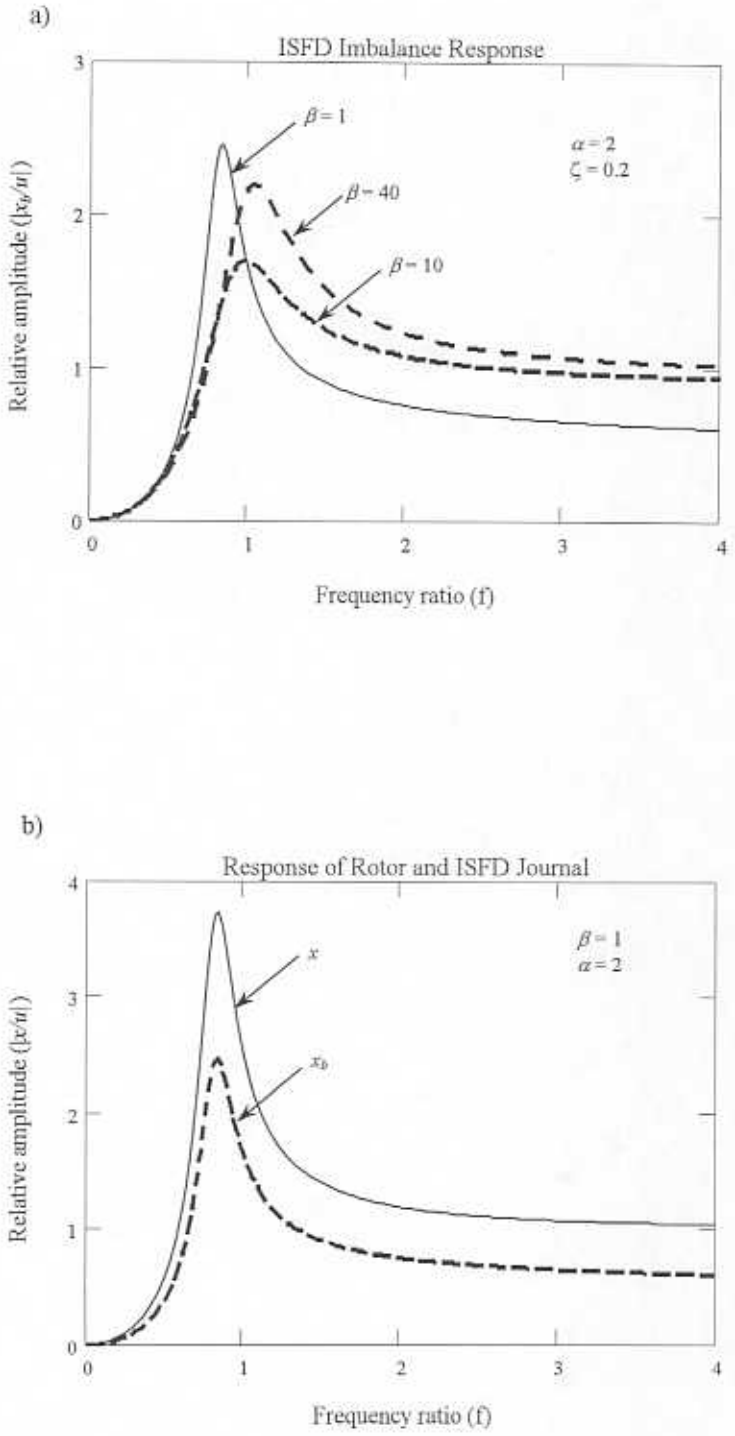

Figure 12. Predicted rotor and bearing amplitude of frequency response.
a) Bearing frequency response amplitudes for different values of bearing to support damping ratio (β)
b) Rotor and bearing response amplitudes for $\beta = 1$

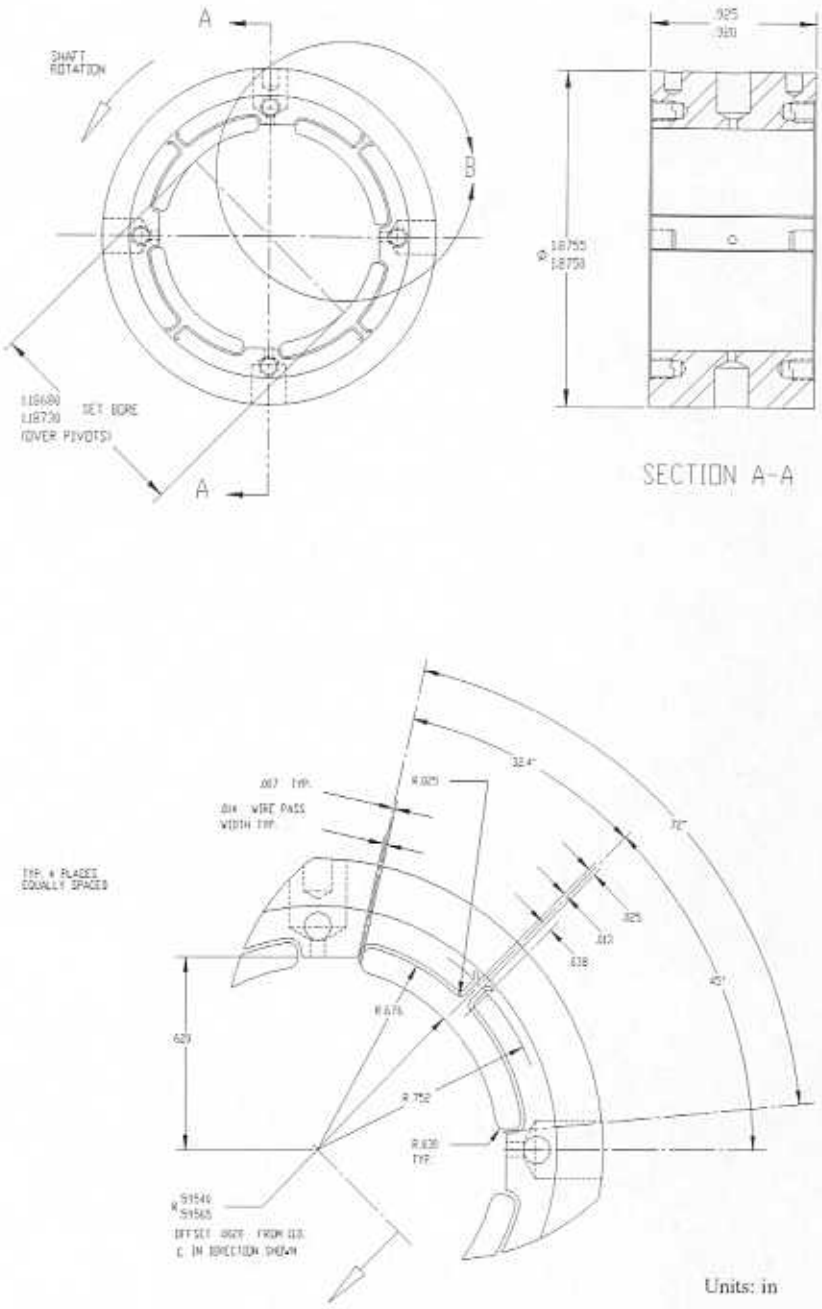

Figure 13. Flexure pivot tilting pad journal bearing lay out and main dimensions.

a)

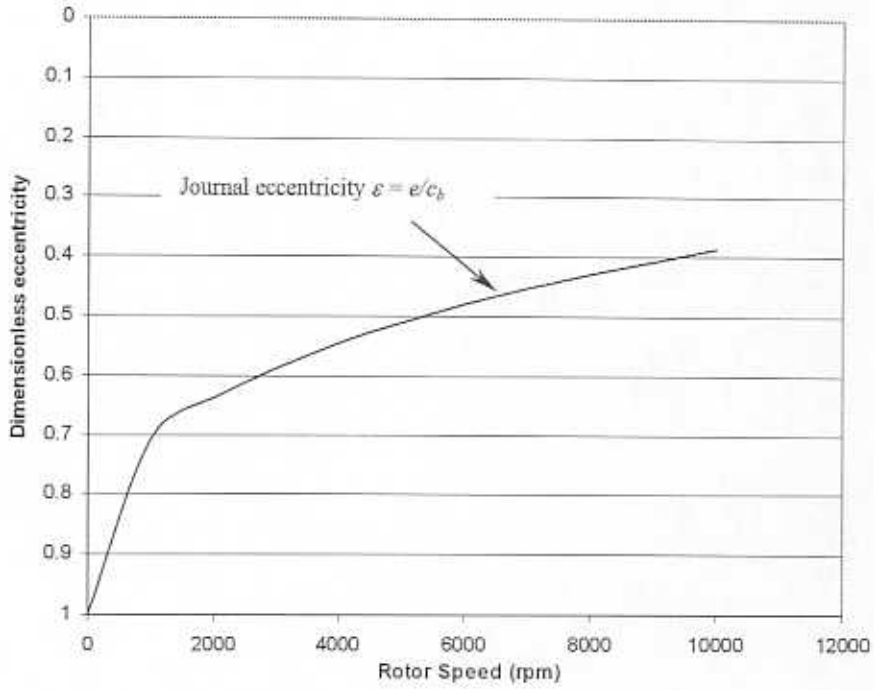

b)

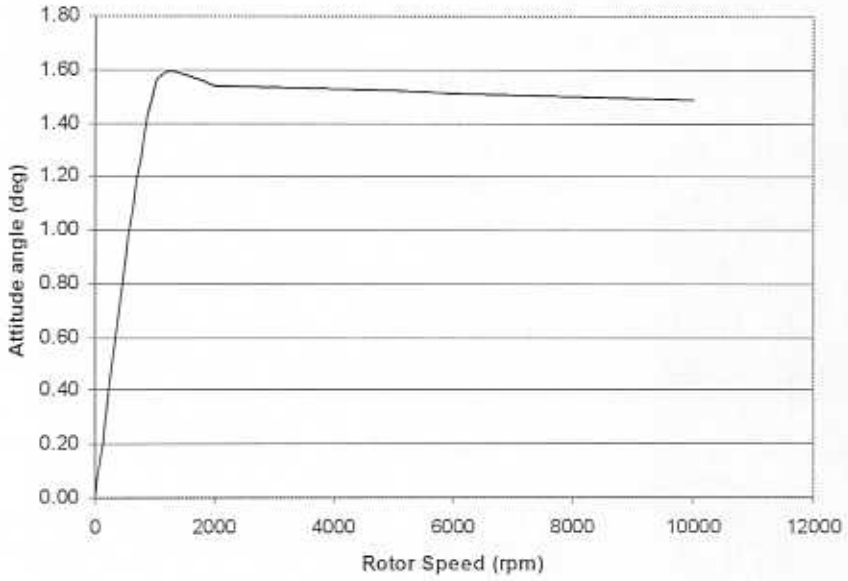

Figure 14. Predicted steady state characteristics of test flexure pivot tilting pad journal bearing. a) Dimensionless journal eccentricity ($\varepsilon = e/c_b$). b) attitude angle.

a)

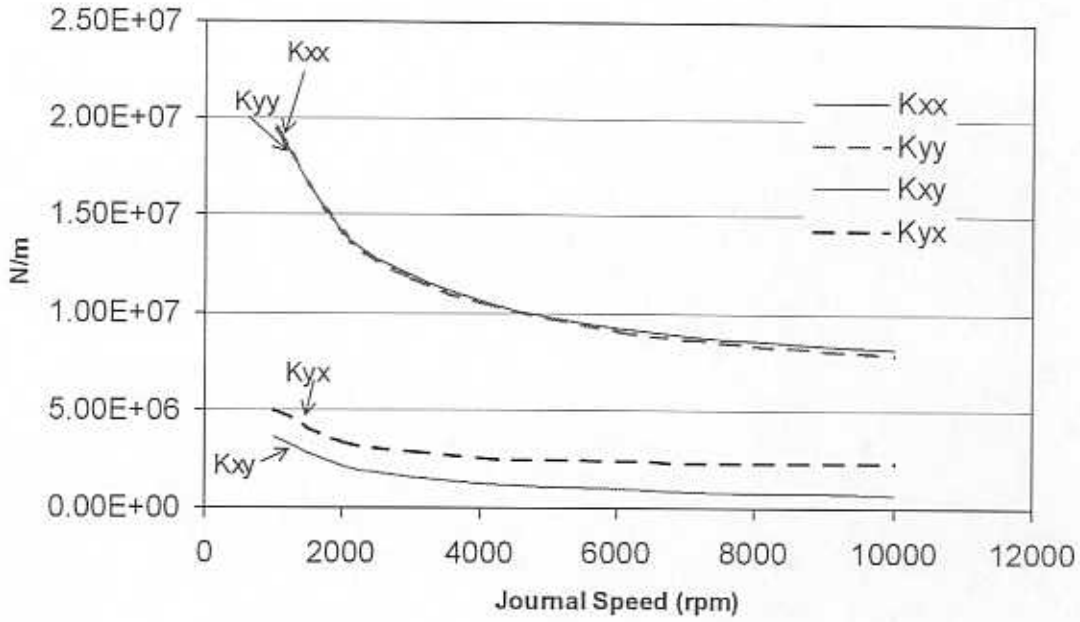

b)

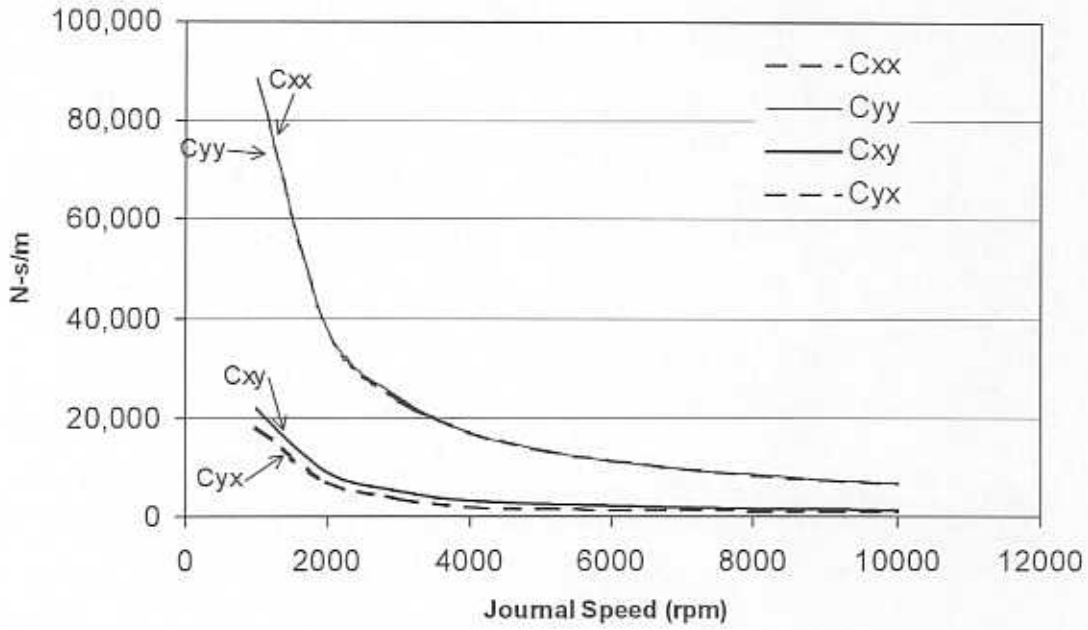

Figure 15. Predicted synchronous rotordynamic force coefficients of test flexure pivot tilting pad journal bearing. a) stiffness coefficients, b) damping force coefficients.

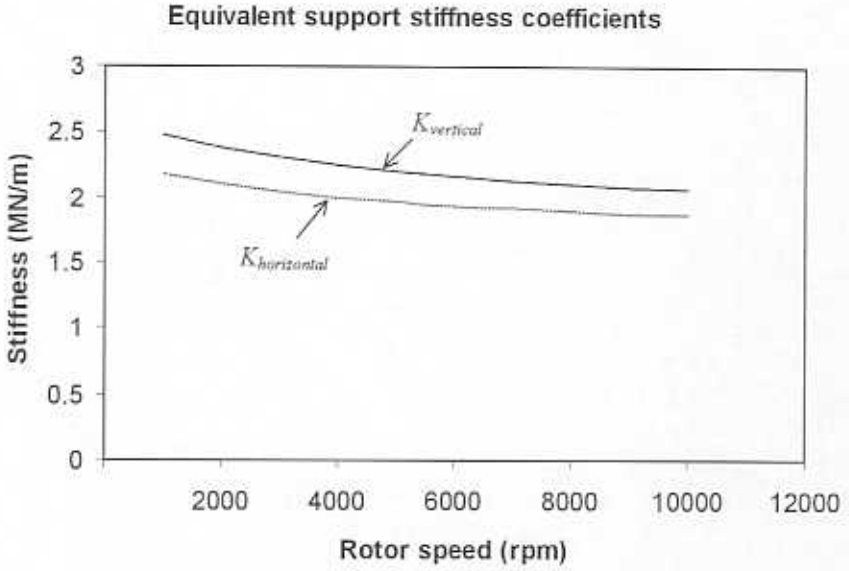

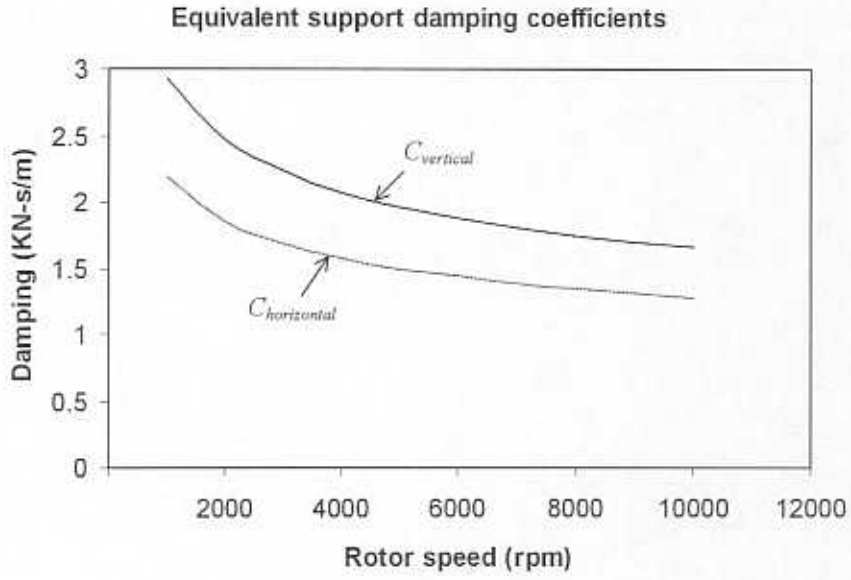

Figure 16. Predicted equivalent *FPJB-ISFD*-pedestal assembly a) stiffness and b) damping coefficients.

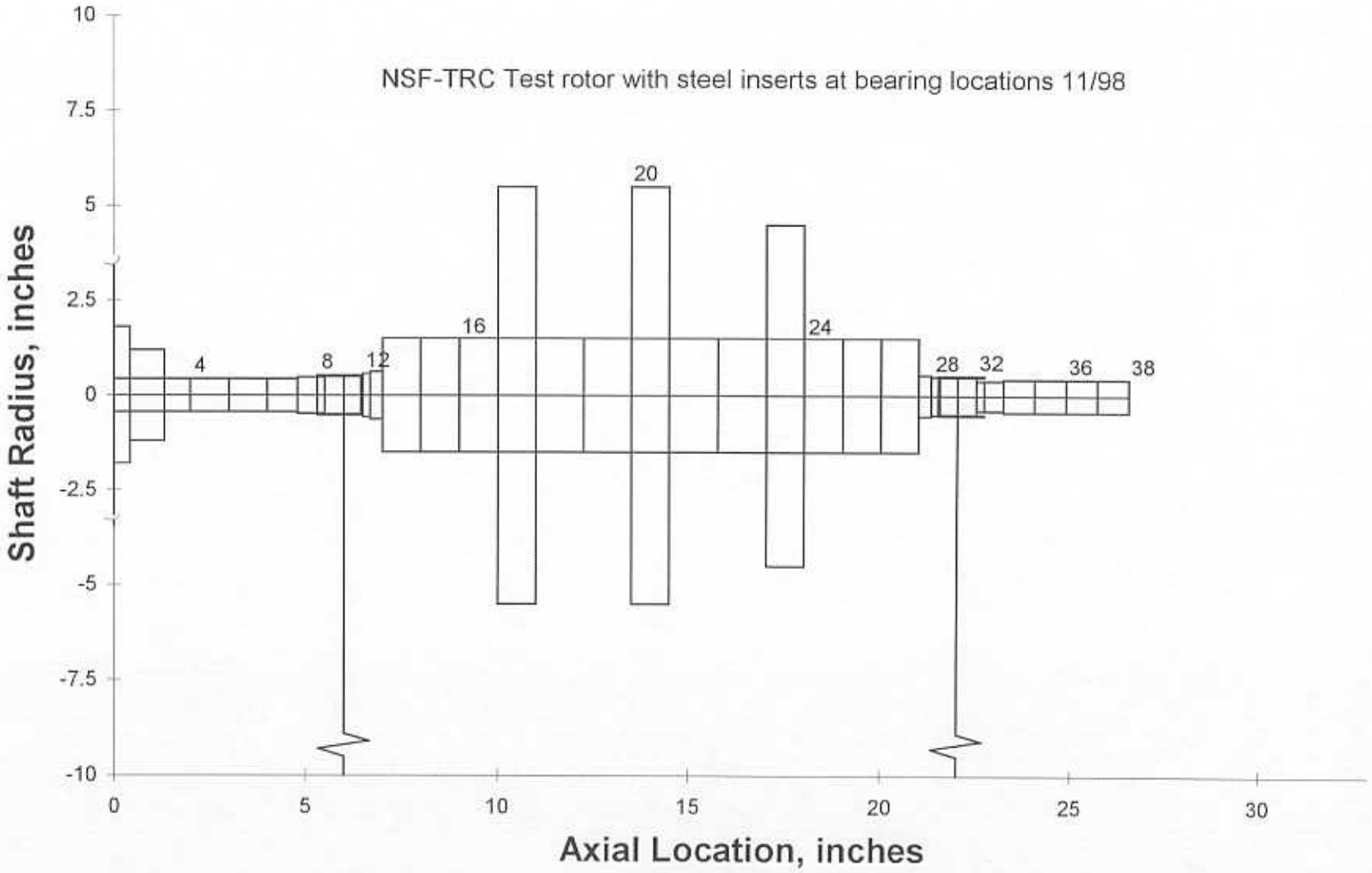

Figure 17. Transfer matrix model for test rotor and supports

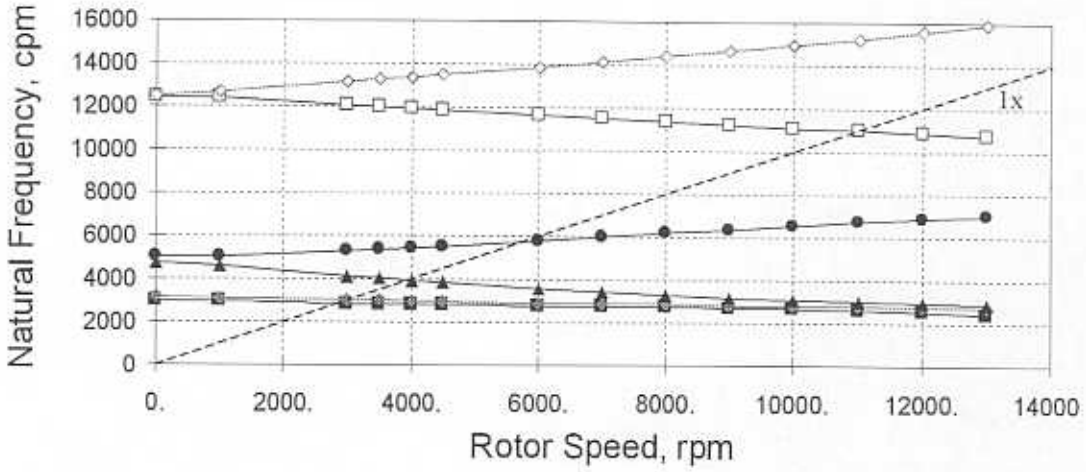

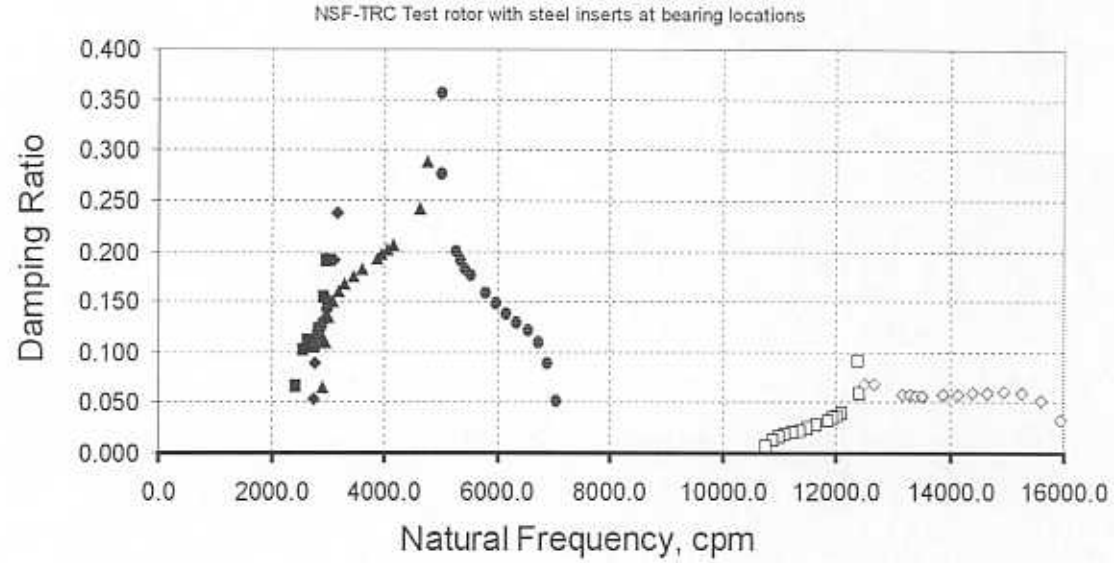

Figure 18. Predicted rotor-bearing system damped natural frequency and stability maps.

a)

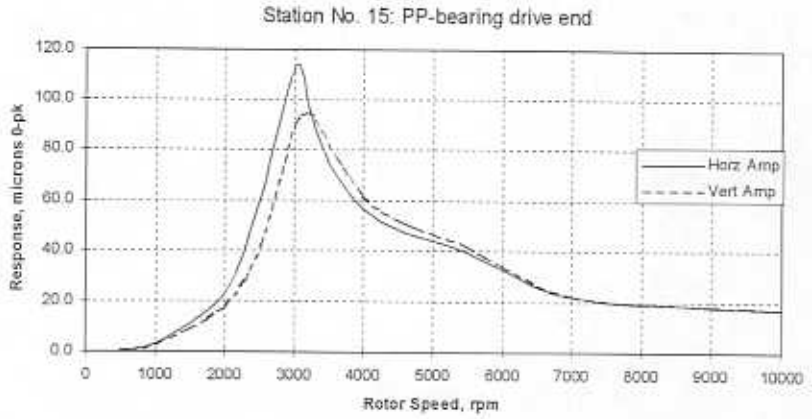

b)

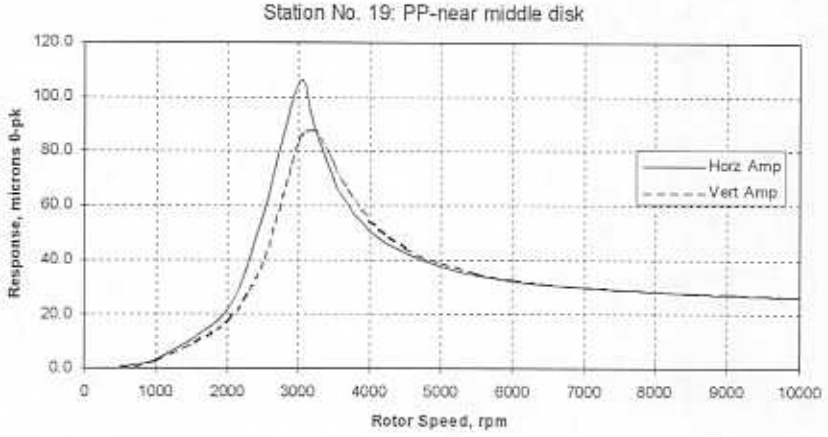

c)

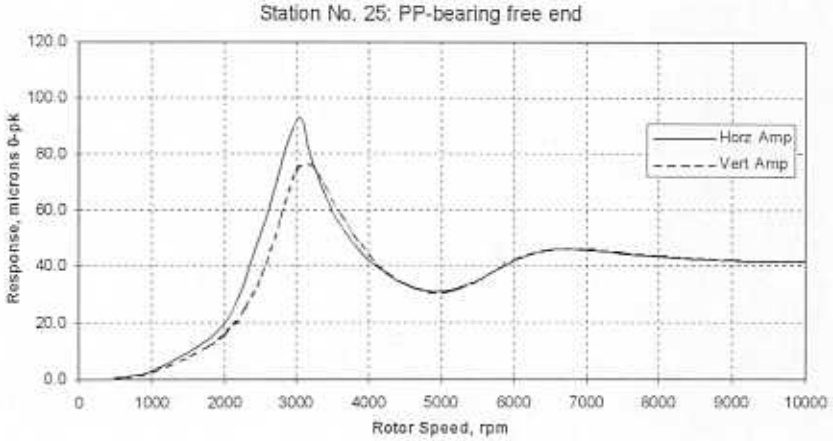

Figure 19. Predicted synchronous response of test rotor to mass imbalance attached at middle disk (45 gr-in) a) Drive end, b) Near middle disk, and c) Free end.

a)

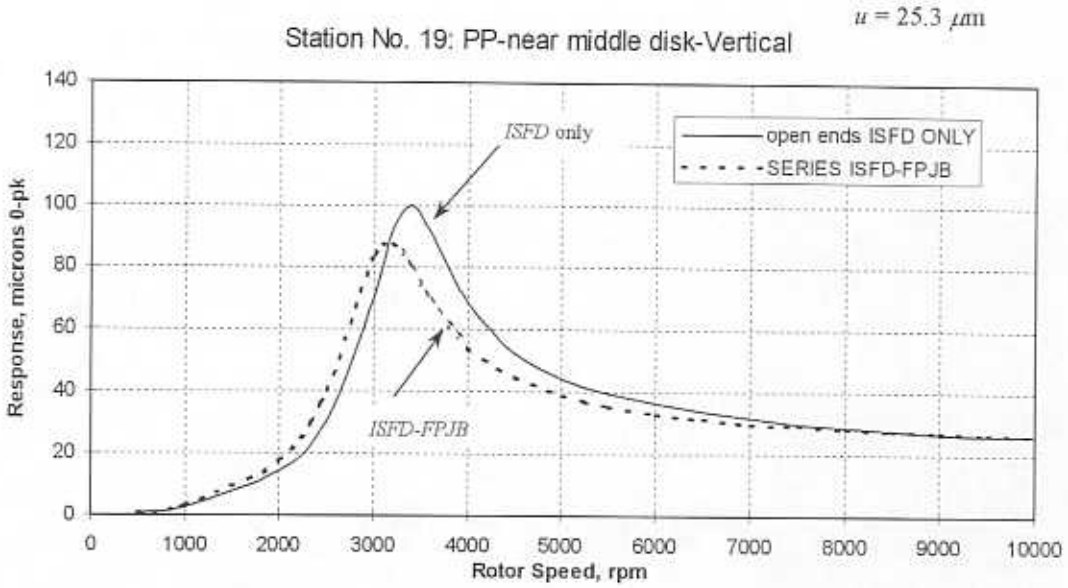

b)

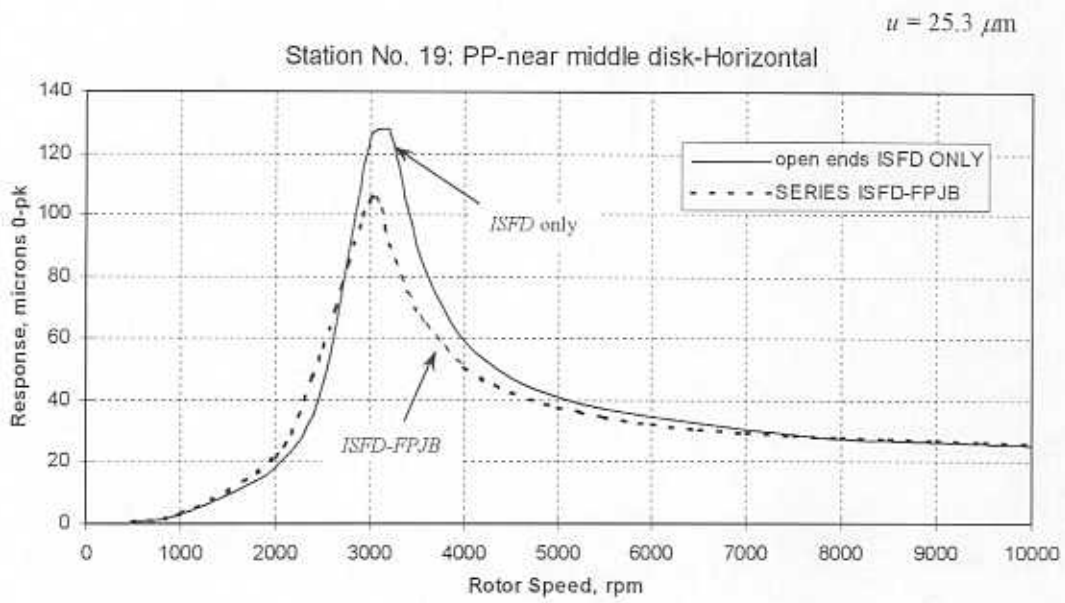

Figure 20. Comparisons of predicted rotor synchronous response to mass imbalance at middle disk (m = 10 gr at r = 114.4 mm, u = 25.3 μm), for two bearing system configurations: *ISFD* only (open ends) and series *ISFD-FPJB* support. a) Vertical direction. b) Horizontal direction.

APPENDIX A. DAMPING FORCE COEFFICIENTS OF A 0.051 MM (2 MILS) END SEALED INTEGRAL DAMPER

De Santiago and San Andrés (1998) detail *impact load* and imbalance response tests conducted on the three-disk rigid rotor supported on end-sealed integral squeeze film dampers (*ISFD*) for end gap clearances of 0.127, 0.102, and 0.076 mm (5, 4, and 3 mils). The measurements indicate that the *ISFD* damping coefficients increase as the end-seal gaps are reduced and without substantial reduction on the damper flow consumption. This appendix presents the experimental results obtained for an end gap clearance equal to 0.051 mm (0.002 inch), and provides comparison with results from previous impact tests for increasing lubricant viscosities.

The *ISFDs* are sealed with an end-seal plate and a calibrated gap equal to 0.051 mm (0.002 in). A detail of the end seal is shown in Figure A1. The steel shims are semicircular in shape and fastened to the damper with the end cover plates. To compensate for a small amount of misalignment in the test rig, one shim of 0.076 millimeters (0.003 in) thickness is located on the top upper half of the outboard face of the free-end *ISFD*.

A load cell hammer is used to impact the middle disk at a location 180° apart from the accelerometer. The impacts are performed on both the horizontal and vertical directions. Lubricant temperature measurements are performed with type-K thermocouples installed in the reservoir and also attached to the side faces of the damper housing.

The structural S-shaped webs of the dampers (see Figure 6 in the main body of this report) as well as custom hose-type seals in the bearing housing provide "dry" structural damping, even without lubricant in the integral dampers. These coefficients must be accounted for in order to identify the damping coefficients provided solely by the viscous forces from the lubricant film. The *ISFD* viscous damping coefficient is calculated by subtracting the dry damping from the overall system damping coefficients determined with lubricant in the dampers. In this process, the assumption is made that the motion of the rotor at the bearings and seal locations is the same, (i. e. cylindrical rigid body mode). This assumption is further verified by the experimental measurements.

Table A1 shows the lubricant (ISO VG 10) viscosity measured at increasing temperatures in a spindle viscometer. Table A2 lists the identified overall system damping coefficients and the estimated *ISFD*

viscous damping coefficients in the vertical and horizontal planes. The identified coefficients are determined from averaged transfer functions obtained from 10 repeated impacts in each direction, vertical and horizontal, and for a range of lubricant viscosities. Figure A2 shows the system viscous damping coefficients to consistently increase as the lubricant viscosity increases. Figures A3a and A3b include the whole set of system damping coefficients for the different end seal gaps investigated. The open ends *ISFD* (i.e. without an end-seal) is shown as the baseline to demonstrate the benefit of end seals in increasing the amount of damping in the rotor-*ISFD* system. The damping coefficients of the current 0.051 mm (0.002 in) end-seal gap show the largest magnitudes. These results are consistent with the prior identified trends.

Figure A4 depicts the measured overall flow rate for the 0.051 mm (0.002 in) end-seal gap as well as the flow rates from prior experiments for larger end seal gaps (De Santiago and San Andrés, 1998). The measurements reveal that the 0.051 mm (0.002 inch) end-seal gap restricts severely the oil flow rate at the test supply pressures. The reference curve for the flow rates corresponds also to the open-ends *ISFD* configuration (i.e. no end seal). The prior measurements show an identical reduction in the flow rate through the damper with end seals, regardless of the end-seal gap clearance. However, the tightest end-seal gap of 0.051 mm (0.002 inch) does not follow the anticipated trend. Presumably, damper journal misalignment or trapped dirt in the seals may have affected the through flow of lubricant in the seals.

Closure

The measurements of the impact response test on a rotor-*ISFDs* system demonstrate that a 0.051 mm (0.002 inch) end-seal gap does render increased damping coefficients. The results complement and validate prior measurements performed with larger end-seal gaps. However, the test end gap seal provides a much larger reduction in through flow rate as compared with earlier experiments performed with larger end gap seals.

Table A.1 Measured viscosity of lubricant (ISO VG 10 oil.

Temperature °C (°F)	Viscosity CentiPoise
22.6 (72.7)	16.06
25.3 (77.5)	13.95
29.4 (84.9)	12.26
34.1 (93.4)	10.14
40.0 (104)	8.45
44.0 (111)	7.65
50.4 (123)	6.54

Specific gravity: 0.85

Table A.2 Damping coefficients estimated from impact tests for different lubricant viscosity. Integral damper with end-seal gap equal to 0.051 mm (0.002 inch).

Dry (structural) system damping coefficient: Horizontal = 1,170.66 N-s/m (23.7 °C), Vertical = 1,710.86 N-s/m (23.5 °C)

Viscous Damping Calculations with 0.051 mm End-Seal Gap – Vertical Direction						
Temperature °C	23.67	27.28	30.28	32.89	35.33	37.72
Viscosity (cP)	15.52	13.81	12.53	11.52	10.64	9.85
Damping (N-s/m)						
Overall system	6,003.0	5,708.1	5,654.7	5,389.9	5,152.2	5,009.6
Viscous	4292.1	3,997.2	3,943.9	3,679.0	3,441.4	3,298.7
Viscous Damping Calculations with 0.051 mm End-Seal Gap – Horizontal Direction						
Temperature °C	23.89	27.61	29.78	32.78	34.89	38.22
Viscosity (cP)	15.40	13.66	12.73	11.56	10.80	9.69
Damping (N-s/m)						
Overall system	4,368.9	4,172.9	3,843.8	3,693.0	3,440.1	3,290.8
Viscous	3,198.3	3,002.2	2,673.1	2,522.3	2,269.4	2,120.1

Note: Viscous damping coefficients are the overall result of the two ISFDs acting in parallel on the rotor supports.

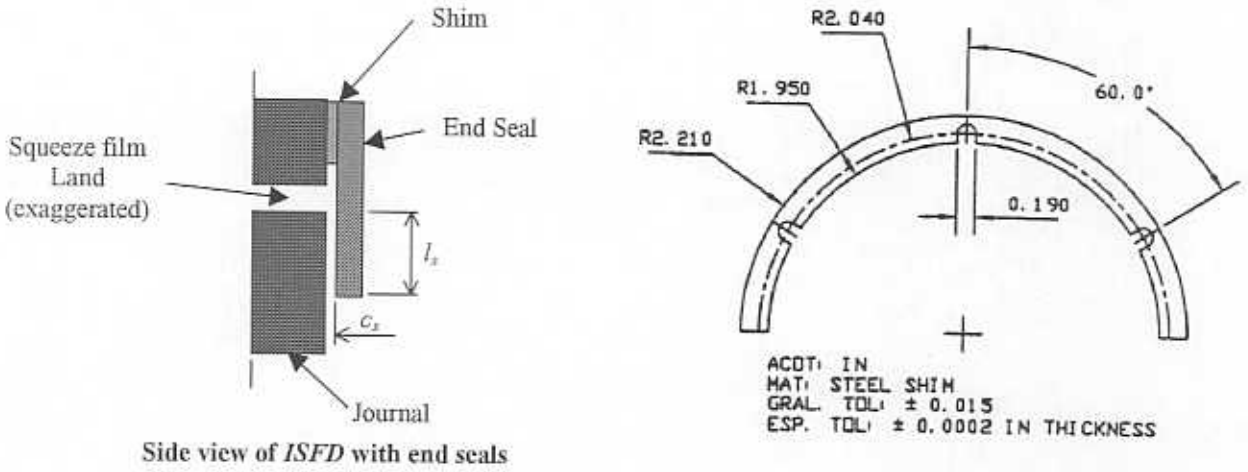

Figure A.1 Calibrated stainless steel stock shim and side view of the *ISFD* with end plate seal.

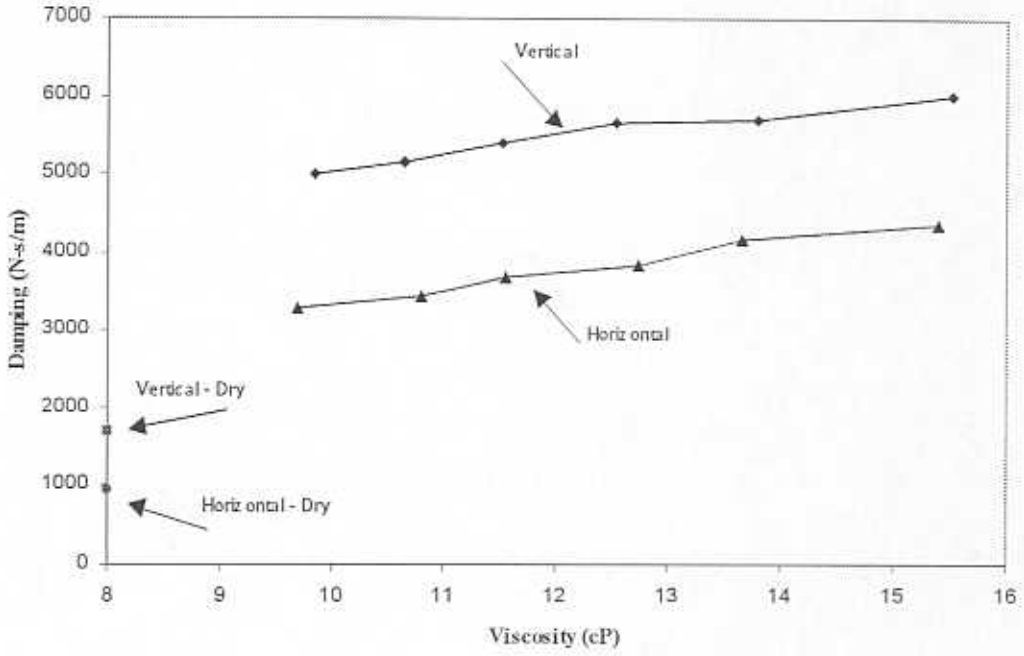

Figure A.2. System damping coefficient from impact tests at zero rotational speed. 0.051 mm (2 mils) end gap seals on integral *SFDs*.

a) vertical

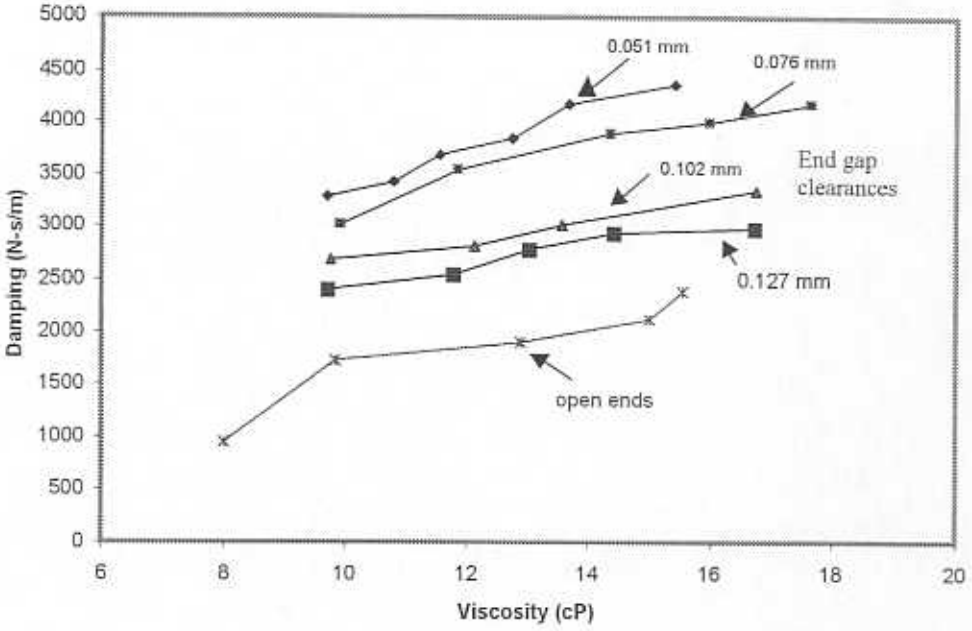

b) horizontal

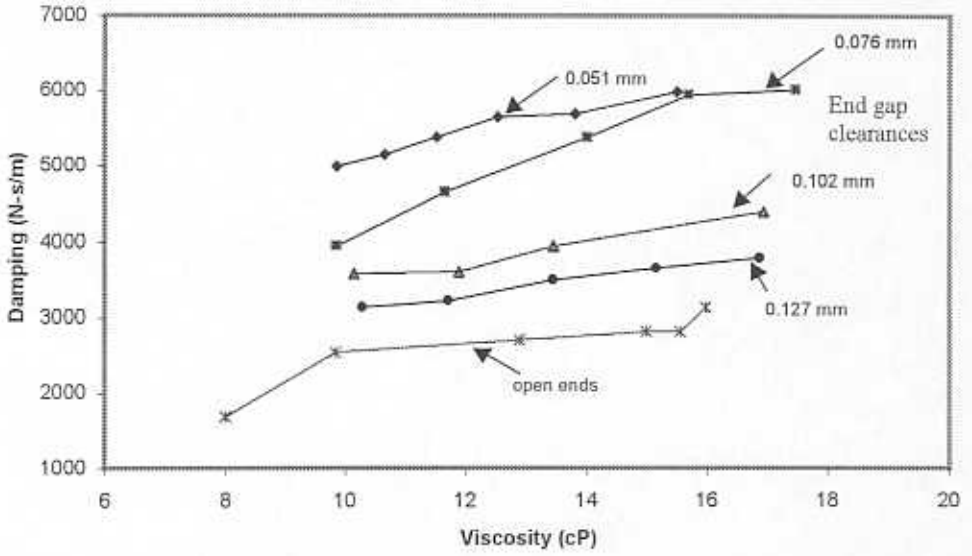

Figure A.3. System damping coefficient from impact tests at zero rotational speed for different values of end seal clearances.
a) vertical direction and b) horizontal direction.

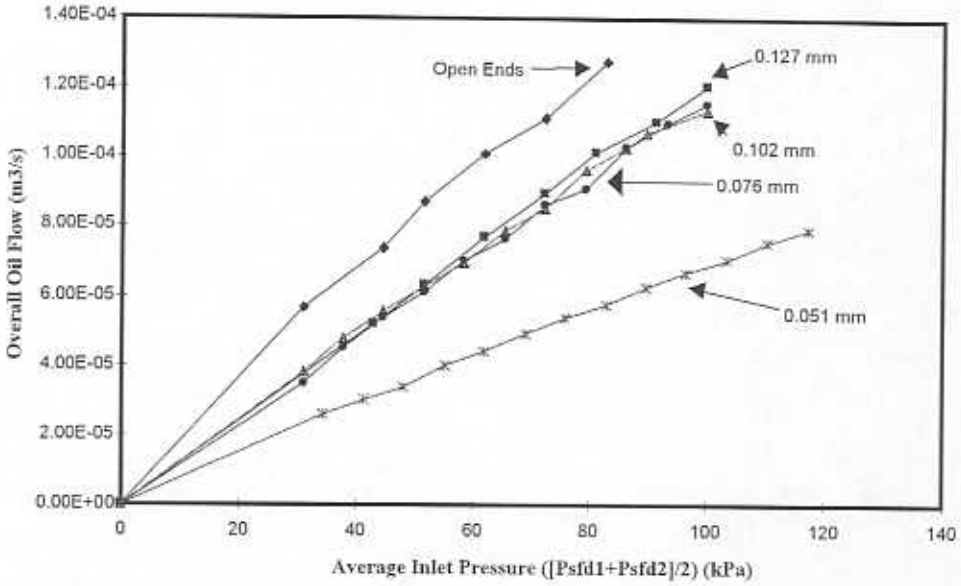

Figure A.4. Experimental oil flow consumption in *ISFDs* for different seal gaps at zero rotational speed.